Quaternary International 694 (2024) 26–50

Contents lists available at ScienceDirect

Quaternary International

journal homepage: www.elsevier.com/locate/quaint

Early Holocene inundation of Doggerland and its impact on hunter-gatherers: An inundation model and dates-as-data approach

P.W. Hoebe [a,*], K.M. Cohen [b], F.S. Busschers [c], S. van Heteren [c], J.H.M. Peeters [a]

[a] Groningen Institute of Archaeology, Faculty of Arts, University of Groningen, Poststraat 6, 9712 ER Groningen, the Netherlands
[b] Department of Physical Geography, Faculty of Geosciences, Utrecht University, Princetonlaan 8a, 3584 CB Utrecht, the Netherlands
[c] Geological Survey of the Netherlands, TNO Utrecht, Princetonlaan 6, 3584, CB Utrecht, the Netherlands

ARTICLE INFO

Keywords:
Sea-level rise
Inundation modelling
Mesolithic
Radiocarbon
Dates-as-data

ABSTRACT

Sea-level rise was a key factor changing environments during the Early Holocene in Northwest Europe. It affected Mesolithic hunter-gatherer communities by inundating large areas in the current North Sea, commonly referred to as Doggerland. In this paper we present novel inundation models for the southern North Sea providing visualisations of lateral inundation driven by sea-level rise and relate it to frequency analysis of radiocarbon dates from archaeological sites. These improve on previous studies that relied on bathymetric data, which includes post-inundation overprints of Holocene sedimentation and erosion, and thus significantly underestimates the timing of inundation in some areas.

We constructed a paleoDEM (a composite elevation grid of the top of the Pleistocene) for the eastern part of the southern North Sea; and sea level surfaces that combine relative sea-level curves from glacio-isostatic adjustment models optimised for Britain and southern Scandinavia respectively. We corrected our paleoDEMs for tectonic background basin subsidence, and in the inundation modelling account for pre-compaction elevation of peat in coastal areas. We evaluated the impact of these model components on our results and describe the possible inundation history of Doggerland. We suggest earlier inundation than predicted by previous models, showing significant area loss around 10.5–10 ka cal BP.

Palaeogeographic changes are compared with archaeological radiocarbon data using a dates-as-data approach. Composite Kernel Density Estimate and permutation tested Summed Probability Distributions are used as a proxy for the visibility, nature and intensity of human activity. Results indicate key periods of growth and decline recorded in the dataset, as well as regional differences in growth rate, some correlating with inundation phases. Chiefly, we find elevated growth rates around 10.5–10 ka in northwest Germany and the Netherlands, contemporaneous with the abovementioned phase of extensive area loss, and moreover, with changes in culture and practices on Early Mesolithic sites.

However, the spatiotemporal distribution of archaeological data is significantly influenced by accessibility and preservation of sediments of a certain age. We discuss the importance of inundation modelling and sediment data in understanding how landscape taphonomy affects archaeological patterning, especially in dates-as-data approaches.

1. Introduction

Early Holocene sea-level rise between 12 ka and 7ka cal BP[1] was a key factor in the changing northwest European environment, ultimately submerging the region now commonly referred to as 'Doggerland' beneath the North Sea (Cohen et al., 2017). Hunter-gatherer communities living in and around Doggerland had to deal with these changes occurring at multiple temporal and spatial scales. Communities were possibly exposed to hazards related to the flooding of large areas, although in other cases changes may have led to new opportunities. Several studies previously attempted to gain insight into the flooding history and potential consequences for the human occupation of Doggerland and surroundings (Fitch et al., 2007, 2022; Sturt et al., 2013; Brooks et al., 2011; Weninger et al., 2008; Behre, 2007; Ward et al.,

* Corresponding author.
E-mail address: p.w.hoebe@rug.nl (P.W. Hoebe).

[1] All dates in this paper are in years or killoannum (ka) calibrated BP.

https://doi.org/10.1016/j.quaint.2024.05.006
Received 28 February 2024; Received in revised form 12 May 2024; Accepted 13 May 2024
Available online 17 May 2024

2006; Lambeck et al., 1998).

Some of these studies are based on intersecting sea-level history (age-depth data on past sea-level positions) with seafloor topographic digital elevation models (DEMs). Such inundation models visualise the lateral inundation driven by vertical sea-level rise, providing palaeogeographic maps useful to archaeologists. However, the spatial and temporal scales of such studies have been relatively coarse, both for the time-steps and control points of the sea-level history and for the topographic data quality and resolution of the DEMs. Sea-level history varies spatially and was obtained from geophysical modelling of ice-sheet mass, ocean volume and land-movement response (glacio-isostatic adjustment; GIA), whereas DEMs were obtained from various bathymetric data (upscaled from original soundings and swath surveys). Scarce geological observational data (sea-level index points, SLIPs; e.g. Shennan et al., 2000, 2018) served as validation data and guided selection of particular GIA model output, noting that GIA-modelling also was going through improvement steps regarding numerical model specification and computation (e.g. Steffen and Wu, 2011). Simplifications were understandably applied in the first generations of inundation models, with inherent problems and limitations to use of the insights at meso and local scale (Vis et al., 2015; Cohen et al., 2014). Consequently, connecting and confronting inundation models with archaeological data was limited to a 500-year to millennial scale with limited spatial resolution. However, to investigate effects of sea-level rise on human behaviour, alignment of patterns in archaeological data with sea-level rise at a 100 to 250-year scale is preferred (Hoebe et al., 2023a; Bailey et al., 2020a).

In this paper we focus on two essential aspects required to understand the impact of sea-level rise on the geography and hunter-gatherer communities. First off, we aim at an improved inundation model (IM) for the southern North Sea at medium spatial resolution (5 × 5 km) to account for small-scale topography, and high temporal (250y steps) resolution, to accommodate archaeological analysis. Second, we explore quantitative relationships between inundation-model outputs with a systematically assembled archaeological radiocarbon dataset (Hoebe et al., 2023a) by means of a dates-as-data approach (Crema, 2022). Compared to earlier generations of inundation modelling, we targeted three improvements.

1) Topographic features in the elevation model of the drowning surface (paleo-relief, paleoDEM) are to be representative for the landscape at the time of drowning. Hereto, present-day bathymetric data are corrected for sedimentation and erosion overprints (superimposed characteristics) synchronous with and post-dating first inundation, hence resulting in an elevation model at the time of inundation.
2) Absolute elevations considering sea-level and land-surface intersection need to be representative of the time of drowning, necessitating sea-level histories and elevation data of drowning surfaces to honour both geological-data insights and modelling-implied spatiotemporally variable glacio-isostasy insights, across the study area consistently.
3) Absolute elevation corrections for other spatially variant subsidence terms are considered. To construct the paleoDEM, we have brought together disparate geological data for sub-seafloor and coastal plain from on- and offshore Belgium, the Netherlands and Lower Saxony. For offshore England such data was not yet available.

To evaluate the effects of paleoDEM-correction and modelling choices on the timing and extent of inundation, we present output at varying quality/accuracy levels of paleoDEM sea level history, and further modelling components.

To use inundation modelling as a means to contextualise changes in human behaviour, time-sensitive archaeological data is required. At this larger regional and temporal scale, a dates-as-data approach permits the exploration of broader changes in overall activity, and potentially demography, in relation to internal (e.g. cultural, social) or external (e.g. environmental) pressures (Hoebe et al., 2023a; Crema, 2022; Crema and Bevan, 2021; Timpson et al., 2014; Shennan et al., 2013). Although the methods available are easily applied to extant radiocarbon datasets, the interpretation of results is difficult, owing to the many potential sources of bias between past reality and dataset formation (research intensity, preservation, data availability), as well as inherent methodological complications (ibid, see also Contreras and Codding, 2023, Carleton and Groucutt, 2021, Ward and Larcombe, 2021, Perreault, 2019: 40–111, Contreras and Meadows, 2014). Dates-as-data approaches have however been much improved by the identification of biases, by model-based testing, and by methodological conceptualisations.

Below, we first address the geological processes relevant to the inundation model: those leading up to the surface situation at the onset of the Holocene, as well as the subsequent marine sedimentary and erosive processes that transformed the sea floor and coastal regions. Also, we provide a brief outline of the broader archaeological context corresponding to the postglacial submergence of Doggerland. The methods section details the process of inundation-model construction and the components therein (elevation models, sea-level rise models, corrections), as well as the archaeological radiocarbon dataset and analytical methods employed. The inundation model and dates-as-data results are presented separately, before we discuss their interrelationships and implications.

2. Regional context

2.1. The North Sea Basin up to the Late Pleistocene

The North Sea Basin and the surrounding regions of Britain and continental Northwest Europe are highly diverse in terms of their geomorphological, substrate and paleoenvironmental characteristics (for a comprehensive overview see Cohen et al., 2017:150–166). The North Sea floor comprises sediments and landforms from the last few ice ages, with older Quaternary deposits sunk deeper. Exceptions are the British near shore and the very southwest of the North Sea (Belgian--French-English waters), positioned outside the subsiding tectonic structure that dominates the southern North Sea Basin (Hijma et al., 2012). Great shallowing of southern and central parts of the basin occurred through the Quaternary, in the last million years to highstand bathymetric depths in the range of 75 to 25 m beneath MSL (Arfai et al., 2018). Simultaneously the amplitude and periodicity of glacial climate and sea-level oscillations increased (e.g. Cohen and Gibbard, 2019; Lisiecki and Raymo, 2005), reaching global lowstands of −90 to −150 m during the coldest periods (e.g. Rohling et al., 2009; Waelbroeck et al., 2002), while the British and Scandinavian ice sheets expanded across northern parts of the North Sea basin. Together, these developments have made sea-level fluctuations expose and inundate the floors of the North Sea, the longer record of which is complicated by subglacial and proglacial landscape evolutionary action and differential preservation bias (Fitch et al., 2022; Cartelle et al., 2021; Gupta et al., 2007, 2017; Cohen et al., 2012; Hijma et al., 2012).

During the Saalian period, the penultimate glacial culminating around 150 ka cal BP, south-westward advance of joint Scandinavian and Baltic ice sheets left prominent ice-pushed ridges, as well as till plateaus in Northwest Europe, including the North Sea (Cohen et al., 2022). During the Weichselian, this process repeated but reached less far south, leaving large complexes of ice-pushed moraines in northern Denmark and the Dogger Bank area (Clark et al., 2022, Emery et al., 2019; Cohen et al., 2017:160). British ice-sheets expanded likewise eastward into the North Sea basin, plastering near-coastal regions such as the Cleaver Bank with till sheets (also in earlier glacial before the Saalian; Lincolnshire and Norfolk: Anglian, Wolstonian and Devensian glaciation episodes) and subglacially carving marked lows (the Outer Silver pit, see Fig. 1; ibid).

Generally, during glacial lowstands, rivers traversed the exposed

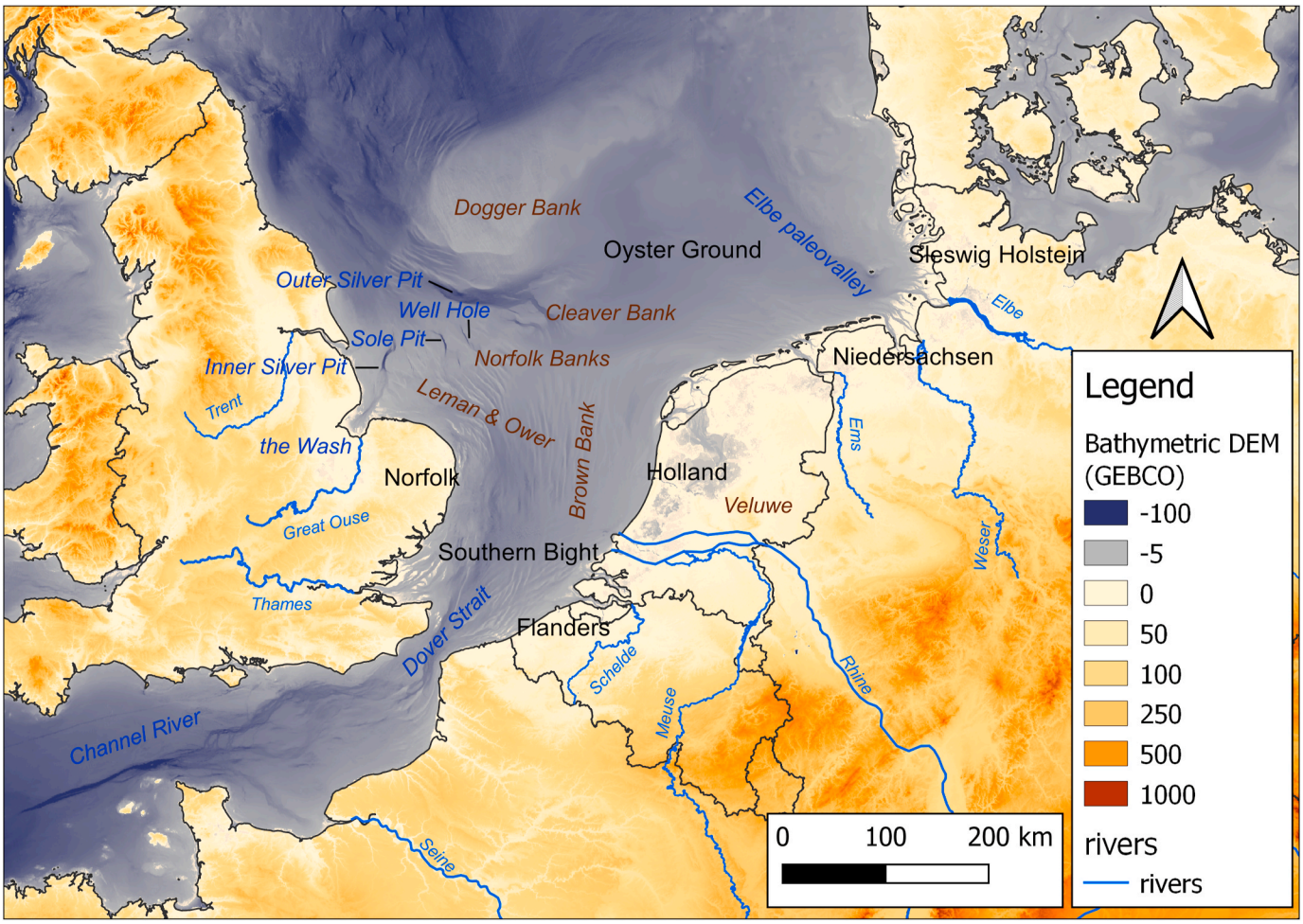

Fig. 1. General Bathymetric Chart of the Oceans (GEBCO) with selected geographic features indicated.

shelf area: ice-marginal outwash rivers fed from along the ice front and periglacial rivers from the south (Elbe, Weser, Rhine, Meuse, Scheldt, Thames). During shorter instances, proglacial lakes appear to have formed, as drainage was blocked by the ice-sheet front along the north, while southerly basin-rim outlets functioned as sills (Cotterill et al., 2017). Under these conditions, ice-marginal discharge was routed south, explaining erosional features of the English-Belgian shelf and Dover Strait, connecting North Sea and English Channel (Clark et al., 2022; Cohen et al., 2017: 158; Hijma et al., 2012; Gupta et al., 2007). At times of deglaciation, meltwater-filled lakes appeared and persisted as depressions in formerly ice-covered areas, while ice-marginal rivers along the retreated ice fronts could reroute. Such rerouting at the end of the Weichselian caused the Elbe ice-marginal system to carve a fairly deep valley (tens of meters deeper than the till and outwash surroundings; Özmaral et al., 2022) into the North Sea floor towards the Norwegian Channel. In periglacial catchment areas to its south, cold climate and established permafrost caused seasonally alternating arid and nival (snowy) conditions, which led to the deposition of a blanket of aeolian deposits (European coversand and loess belts; e.g. Lehmkuhl et al., 2021: 5–23, 30; Vandenberghe in Schaetzl et al., 2018:592–93). Winter-time dry and barren riverbeds and floodplains formed important source areas for silt and sand, picked up by wind. Aeolian deposition was particularly intense between 35 and 11.5 ka, when a series of climatic cold spells, owing to North Atlantic disruptions in thermohaline ocean circulation (stadials), affected the then-existing tundra-polar desert biomes of the North Sea area.

During interglacials, ice-sheets receded and sea levels rose approximately to modern levels, with marine transgressions causing both erosion and sedimentation (Bailey et al., 2020a; Cohen et al., 2017:156, 2012). Generally, interstadials saw deltaic coastal plains with both riverine and marine sedimentation. This alternating depositional and erosional geological history left a geomorphological 'fingerprint' in the bathymetric data of the North Sea floor, although masked and smoothened by Holocene sea-floor dynamics. Marked regional features (see Fig. 1), besides the aforementioned Elbe valley, are the long and narrow sand banks of the Southern Bight (Holocene tidal currents and wave action interacting with Pleistocene and older substrate; see Laban et al., 1984), the plateau of the Dogger Bank in the Central North Sea (Fitch et al., 2005, 2022; Phillips et al., 2018), as well as carved elongated depressions of subglacial origin, such as Silver Pit, Sole Pit, Well Hole and the particularly large and deep Outer Silver Pit (80 m; Fitch et al., 2022; Briggs et al., 2007). This said, large areas of North Sea bathymetry also appear as flat, shallow and relatively featureless, e.g. the Oyster Grounds (Late Pleistocene lowland, in part covered by Holocene marine deposits; De Haas and Van Weering, 1997)

The above offshore Pleistocene geomorphic review can be extended to the near-shore of the modern coasts and Holocene-buried surfaces in the substrate of the coastal plain. While towards the east and southeast (Denmark, German Bight, Netherlands) this is characterized by low-gradient terrain with Middle and Late Pleistocene glacial landforms dissected by river valleys, towards the west (Britain: Lincolnshire and East Anglian coasts), cliffs developed in Pleistocene till units covering much older Mesozoic bedrock, that also subcrops below abrasion platforms in front. The boundary between these two geomorphic terrains lies in the offshore of the North Sea, where it runs NNW-SSE from the Outer Silver Pit to the Dutch-Belgian coastal borderland (Cohen et al.,

2014, 2017; Hijma et al., 2012)

2.2. Postglacial North Sea transgression

Inundation of the North Sea basin commenced around 22-19 ka when ice sheets began to melt (Clark et al., 2022; Carlson and Clark, 2012) by the end of the global last glacial maximum (LGM). Following this, during 'Termination I', the North Sea and global sea-levels would rise particularly rapidly in the Late Glacial and Early Holocene (14.5–11.7 ka, respectively 11.7–8.2 ka). The sea-level history has a gradual component due to the direct release of meltwater from retreating ice fronts at different locations in the world, but was punctuated by pulsed meltwater release events (Carlson and Clark, 2012) that in sea-level rise reconstructions show up as accelerations and following decelerations (Lambeck et al., 2014; Hijma and Cohen, 2010; Fairbanks, 1989).

The spatial transgression history of the North Sea, i.e. the horizontal inundation, is a function of (1) the rates of sea-level rise (affected by regional subsidence processes besides global ice volume-melt and ocean-volume increase), and (2) the topography at the end of the Pleistocene (see 2.1). Early Holocene transgressed relief differs significantly from the current bathymetric and terrestrial relief in key areas where later sedimentation and/or erosion took place (see 3.1.1, Fig. 3b). Closer to present-day shores, non-marine sedimentation and erosion also took place before areas were transgressed, e.g. by fluvial and aeolian processes (e.g. Abegunrin et al., 2023; Hijma et al., 2012). Furthermore, sedimentation and erosion caused by transgression led to significant overprints of the Late Pleistocene surface, such as Dogger Bank, Outer Silver Pit, Norfolk and Cleaver Bank, the Elbe palaeovalley (see 2.1), as well as building up the coastal plains and isles and shoals of Schleswig Holstein, Niedersachsen, the Netherlands and Flanders. Here, transgression and highstand marine, fluvial and biogenic processes accreted considerable volumes of Holocene sand, clay and peat (see 3.1.1 and 3.1.4 for relief maps), deposited in layers of variable thickness and composition. Locally the Holocene sequence can be 20 or even 30 m thick, especially at the position of the modern coast, thinning landward to near-zero at the inner coastal-plain edge. Along these coasts considerable erosion occurred at the positions of (former) inlets and rivers. Going offshore from the modern coastline, Holocene formations become thinner and generally do not exceed 5 m. Where the Holocene of the coastal plains is predominantly a burying package (fluvial and tidal basal reworking of Pleistocene subcrop occurred locally only), that of the offshore over larger parts of the North Sea is a reworking unit (TNO GDN, 2023). Seafloor sandwave fields originate from remodelling sandy Pleistocene submerged topography. That said, considerable areas of Pleistocene surface have also been preserved below Holocene transgressive deposits, notably over topographic lows in the surface.

As the Holocene sea level rose, so did the groundwater-tables in coast-adjacent regions, owing to riverine base-level grading and capillary effects. In fact, it is groundwater-table rise that causes paludification (conversion of dry to wetland) of regions, in advance of sea-level-driven transgression (Cohen, 2005; Van de Plassche, 1982; Jelgersma, 1961, 1982). This is evidenced by patchy occurrence of so-called basal peat of Early Holocene age (older than 8.5 ka) in offshore areas and the occurrence of basal peat of Middle Holocene age (8.5–4.2 ka) in nearshore areas. These peats began forming in freshwater swamp and fen-bog environments, which transformed into marshes just prior to marine inundation and transgression. In sea-level reconstruction applications, the surface elevation of basal-peat marsh at the time of drowning is considered to correspond to contemporary mean high-water level (Hijma and Cohen, 2019), which for the meso-tidal North Sea was decimetres to 1.5 m above mean sea level (Van Der Molen and De Swart, 2001). The offshore and near-shore basal peat was subject to erosion where continued transgression resulted in wave action along the coasts. This left an uneven patchwork of preserved basal peat deposits. Basal peat occurrence also extends to below the coastal plains, where it was superseded by backbarrier tidal inundations and younger phases of coastal peat formation. During Middle Holocene stages of transgression, when sea-level rise slowed down and the backstepped coastline position began to stabilise in coastal barrier systems, tidal inlets, river mouths and estuaries evolved and occasionally shifted in position (Pierik et al., 2023; Vos et al., 2015; Hijma and Cohen, 2011). This led to further burial and erosion of the originally transgressed surfaces.

An important factor when describing Holocene North Sea inundation geographically is the lateral transgression rate. Because the Early Holocene rates of sea-level rise were higher than later on (judging from global deglaciation reconstructions; e.g. Lambeck et al., 2014), inland shifting of the coastline at this time as geologically recorded in offshore areas, was more rapid than later on. In general (Cohen et al., 2017: 167), Early Holocene transgressed topographic lows (e.g. valley floors and sides) would be expected to preserve the original surface better (intact soils below basal peat bed) than the surfaces of their interfluve areas (basal peat and soils decapitated by marine ravinement action).

2.3. Archaeological context

The North Sea was first identified as a region of interest for submerged archaeology in the 19th century with observations of tree stumps in the intertidal zone along the English coast, and the find of the Leman and Ower Bank harpoon (for recent overviews see Walker et al., 2022; Bailey et al., 2020a; Peeters et al., 2020). Over the past century, more finds were dredged up from the seabed, or caught in fishing nets (Louwe Kooijmans, 1971). In the last 25 years, since the keystone publication by Coles (1998), several research projects have been conducted to contextualise these finds by the mapping and reconstruction of submerged prehistoric landscapes (Walker et al., 2022; Van Heteren et al., 2014; Gaffney et al., 2007). This work initially focussed on the inundation history and changing palaeogeography (Sturt et al., 2013; Gaffney et al., 2007). More recently efforts gear towards environmental studies (Gaffney and Fitch, 2022) and the analysis of an increasing body of archaeological and palaeontological finds (Bailey et al., 2020a; Peeters et al., 2020).

For the northwest European Late Palaeolithic and Mesolithic, the centrally situated North Sea forms a tantalising gap because of the relatively low availability of data on the one hand, and its high preservation potential on the other. Before North Sea finds became more prevalent, this centrality was already attested by the well-established links between Britain and continental Europe, based on typological and technological characteristics of stone tool assemblages from the onshore record. Evidently, the large stretches of back-barrier inland and postglacial coastal areas, nowadays hidden under the North Sea, were inhabited by hunter-gatherers of different cultures or traditions (Momber and Rich, 2015; Peeters and Momber, 2014). Post-LGM hunter--gatherer groups of the Magdalenian (ca. 15 ka), and successive Hamburgian cultural traditions pioneered in areas on either side of the North Sea (Ballin, 2018; Maier, 2015; Pettitt and White, 2012). Contemporaneous similarity in material culture and technology across Northwest Europe persists throughout the Late Glacial and well into the Early Holocene representing the Federmesser Gruppen (Allerød), Ahrensburgian/Long Blade (Younger Dryas - Preboreal), and Early Mesolithic Maglemosian (Preboreal, Early Boreal) traditions. Changes in the intensity of human activity based on radiocarbon date densities (Hoebe et al., 2023a; Mithen and Wicks, 2021; Van Maldegem et al., 2021; Robinson et al., 2013) and regional diversification in northwest European Mesolithic material culture have been established for the 11th and 10th millennium cal BP, and are often discussed in the context of contemporary inundation of Doggerland or climatic cooling events (Conneller, 2021; Crombé, 2019; Conneller and Overton, 2018; Sørensen et al., 2018; Deeben and Niekus, 2016b; Waddington, 2015). However, chronological correlation of specific climate cooling and marine transgression events with changes in the archaeological record remains difficult and complicated by various taphonomic and

methodological issues, which are explored below (3.2, 5.2).

The North Sea archaeological record complements the onshore record mainly with its high preservation potential for organic remains, which are rare in terrestrial contexts (Bailey et al., 2020b; Jöns et al., 2020; Peeters et al., 2009, 2019, 2020; Pieters et al., 2020). The North Sea record spatially varies in age, abundance and preservation potential. These factors depend on the density of past human activity on the one hand and taphonomic processes of sedimentation, erosion and reworking on the other hand (Ward and Larcombe, 2021; Perreault, 2019). While erosion can destroy or displace remains, it can also expose and make contexts of a certain age available to be discovered, which otherwise would remain hidden beneath meters of sediment. North Sea Mesolithic finds stand out for their good preservation, notably of organic materials such as bone and antler. For instance, numerous human skeletal remains contain aDNA, permitting genetic studies at the individual and population scale (Posth et al., 2023; Van der Plicht et al., 2016). Importantly, the vast body of archaeological remains corresponding to the Early Holocene drowning of Doggerland now permits in-depth studies of human responses to this inundating landscape (Peeters et al., 2020).

This stands in contrast with the still limited and sparse evidence for Late Palaeolithic hunter-gatherer activity from the North Sea. Sites assigned to the Magdalenian, Hamburgian and Ahrensburgian cultural traditions are rather dispersed in space, and relatively small in terms of material debris left at dwelling locations. This affects discovery chance, explaining the lack of North Sea finds securely attributed to these cultural traditions. Typically, Federmesser Gruppen sites are very abundant on both sides of the North Sea (Deeben and Niekus, 2016a; Pettitt and White, 2012; Street et al., 2002) and usually consist of dense artefact scatters over larger areas, comparable to what we see for the Mesolithic. The discovery of several finds from the North Sea itself securely dated to the Federmesser period (i.e. Allerød, ca 14-13 ka; Amkreutz et al., 2018; Van der Plicht et al., 2016) may be a reflection of a higher discovery chance. The palaeontological record shows a comparable picture. Radiocarbon-dated faunal remains demonstrate an abundance of pre-LGM and Holocene evidence (Van der Plicht and Kuitems, 2022; Van der Plicht et al., 2016). Harsh polar desert conditions (Van Geel et al., 2024) and great burial depths of contemporary river corridors (Hijma et al., 2012; Busschers et al., 2007) can explain the relative lack of Southern North Sea animal fossils from during the LGM. It remains unclear how to interpret the apparent scarcity of Late Glacial faunal evidence from the North Sea (Van der Plicht and Kuitems, 2022; Van der Plicht et al., 2016) compared to relative abundance of horse and reindeer as seen at onshore sites (Street et al., 2002).

3. Materials and methods

To investigate the impact of marine transgression on human habitats in the North Sea region, we ran and compared inundation models (IMs) at several quality levels (sections 3.1 and 4.1). These quality levels through stepwise inclusion (Fig. 2) relate to the three improvement components declared in the introduction. This way we can compare visualisations at different quality levels encountered in the literature. The spatial and temporal inundation model output is confronted with both the spatial and temporal patterning of archaeological radiocarbon data by means of a dates-as-data approach (sections 3.2 and 4.2).

3.1. Inundation modelling

To assemble input for inundation modelling and run inundation models, we combined and processed data in R and QGIS, using python scripts to automate raster calculator output (Fig. 2, see SI-1 for workflow). The input of each inundation model is a DEM in raster format (section 3.1.1), which is intersected by a sea-level value (SL) drawn from a sea-level model (ESL or GIA) (section 3.1.2). For the highest quality levels, we deploy further DEM corrections (C) for basin background subsidence and modification of the modelled land-water boundary with a correction vector for coastal peat (section 3.1.3).

The overall procedure for each timestep is one of adding, subtracting, and categorising (raster cell) values for DEM, SL and C, giving a time series of raster outputs with the same resolution as the DEM input. Where the DEM (or DEM + C) is lower than the timestep's (local) sea-level value, it is categorised as water, and where it is higher, as land. Ribbon areas considered to be tidally exposed (T) and coastal peat land (P) zones are defined based on relative elevation offsets of 2 m below and above coastline (see section 3.1.4). Having the tidal zone implemented accounts for the absence of explicit post-inundation marine sedimentation in the model. Having the peatland zone implemented accounts for graduality of the transgression process of dry land first transforming into marsh before fully drowning (paludification).

As post-processing of the inundation modelling output rasters, palaeo-coastline maps were compiled, giving insight into spatial differences in the timing of inundation and coastline stability. Last but not least, grid-cell counts for the inundated area per timestep were summarised in histograms, allowing for a more quantitative comparison between models.

3.1.1. Digital elevation models

Inundation studies have often used bathymetric DEMs of the present-day seafloor as their basis for modelling the timing of coastline changes

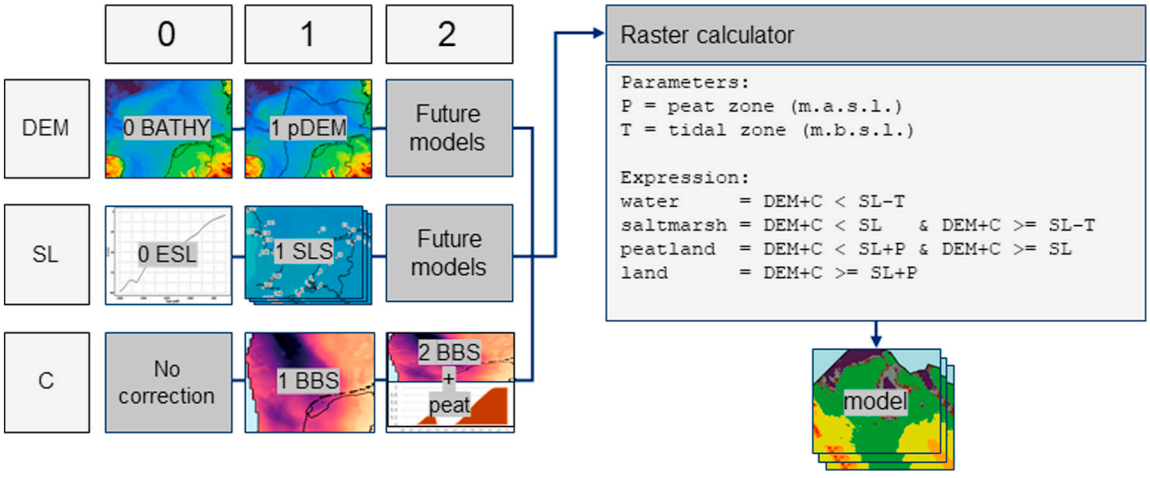

Fig. 2. Inundation model component quality matrix (left) and basic format for output generation for each timestep in the GIS raster calculator. These calculations are done for each timestep for each model configuration (SI-1).

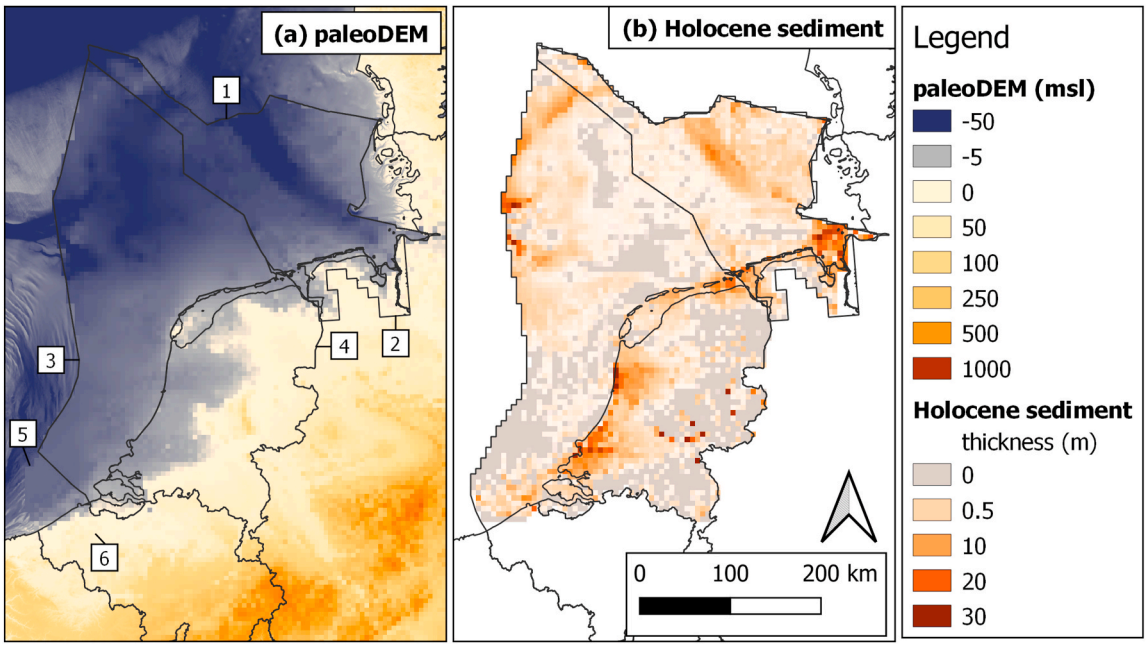

Fig. 3. a) Multi-source compiled paleoDEM (this study; 5 × 5 km); numbering corresponds to the sources in Table 1 b) the difference between the GEBCO DEM (Fig. 1) and the paleoDEM (a), giving the Holocene sedimentation thickness.

(Sturt et al., 2013; Brooks et al., 2011). The General Bathymetric Chart of the Oceans (GEBCO) provides aggregated continuous bathymetric DEMs with worldwide coverage, based on sonar and seismic offshore, complemented with onshore lidar data (download.gebco.net). This is an excellent, ready-made relatively high-resolution resource, but the drawback for using this as a DEM in inundation modelling, is that this includes unwanted overprints of sedimentation, erosion and human action postdating the finalisation of the Pleistocene surface, most notably at the modern coastline and the Holocene coastal plains (Section 2).

To more accurately model inundation, the post-transgression depositional and erosional overprints should be stripped and repaired ('patched'), to convert bathymetric source data to a more representative DEM at the time of inundation (a paleoDEM). For the North Sea basin it is now possible to formulate and apply such patches, aided by geological insights and data, albeit with differing data availability per country and economic use sector, as well as differing decisions for onshore and offshore subareas. For some offshore areas, one may decide to smooth bathymetric sand wave relief attributed to post-transgressive reworking of originally Late Pleistocene periglacial river and aeolian dune-form blanketed terrain. For other offshore areas, one may fall back to national geological datasets that provide depth and burial depth information on locations where the transgressed surface is preserved (e.g. basal peat retrieved in boreholes: Bungenstock et al., 2022; Vermeersen et al., 2018; Koster et al., 2017; or seismic mapping of the Pleistocene-Holocene boundary Van Heteren et al., 2014). For other areas, recent geological survey mapping stimulated by demands from competing economic uses of the sea floor, may provide digital contour-line or raster data for 'top Pleistocene/base Holocene' surfaces.

In this study we constructed a new composite grid of the top of the Pleistocene (m -MSL) for the southern North Sea, incorporating data from the onshore and offshore regions of the Netherlands, Lower Saxony and Belgium. Table 1 lists the resources used to combine in the paleoDEM assembled for this study. Depending on the area, we used stratigraphic point data from boreholes, contour lines and/or grids (see SI-2 details on construction process). Using such a geological mapped surface as a paleoDEM (Fig. 3a) is an improvement upon using a bathymetric DEM (Fig. 1). Calculating the difference between bathymetric DEM and the paleoDEM results in a sediment thickness raster, showing where the difference of DEM choice matters relatively more (Fig. 3b). Onshore it is marked for the Dutch coastal plain and German Ems and Weser estuaries. Offshore it is marked for the Elbe palaeovalley, the southeast-facing flank of the Dogger Bank, and by the rims of Outer Silver Pit.

We note that a paleoDEM is not a perfect reflection of the pre-transgression surface: (1) As it was assembled at a cell size of 5 × 5 km, it smoothed and hence masked microtopography, and (2) it contains data-sparse (due to relatively lower surveying intensity) and data-void areas (due to erosive younger features such as tidal inlets) where interpolation algorithms further smoothed the paleoDEM. Also, (3) it gives the topography upon which several decimetres of thickness of peat

Table 1
Source, coverage, and resolution (x, y) of the different DEMs used in inundation modelling.

	Source	Coverage	Resolution
Bathymetry and DEM			
	General Bathymetric Chart of the Oceans GEBCO (download.gebco.net)	Worldwide	1m, 250 × 250m
paleoDEM			
1	Geopotenzial Deutsche Nordsee GPDN (www.geopotenzial-nordsee.de)	Niedersachsen offshore	2m, isopach
2	Niedersächsischen Bodeninformationssystems NIBIS (nibis.lbeg.de)	Niedersachsen onshore	2m, isopach
3	Offshore mapping programme TNO (FSB this paper, SI-2)	Netherlands offshore	1 cm, 100 × 100m
4	Rijksdienst voor het Cultureel Erfgoed RCE (www.cultureelerfgoed.nl)	Netherlands onshore	1 cm, 100 × 100m
5	Drowned Landscapes of the Belgian continental Shelf De Clercq (2018), De Clercq et al. (2016)	Belgium offshore	1 cm, 100 × 100m
6	Databank Ondergrond Vlaanderen DOV (dov.vlaanderen.de)	Belgium onshore	1 cm, 100 × 100m

formed during centuries just before actual drowning (section 2), so that exact matching of a sea-level position may require applying an offset to account for this (section 3.1.3).

3.1.2. Sea-level histories

Two quality levels of prescribing sea-level rise to the inundation model are used (Fig. 2). The first, lowest quality one is to directly use a generally accepted global 'eustatic' sea-level reconstruction (ESL; taken from Lambeck et al., 2014). Eustatic sea-level history (ESL) mirrors the global ice-sheet history, and in its simplest approximation assumes an even distribution of the meltwater across the ocean surface (i.e. neglecting processes such as self-gravitation; Shennan, 2018). Reconstructing and validating worldwide ice-sheet history and ESL is important for global palaeoclimatic and environmental modelling (Shennan, 2018; Lambeck et al., 2014), but drawing values from ESL reconstructions for regional inundation studies has pitfalls. Instead, relative sea-level histories (RSL) that include imprints of land movement such as subsidence owing to GIA and the basin setting of the North Sea, provide a more relevant approximation. Hence, as two higher-quality sea-level histories, we use reconstructions of regional RSL rise for the North Sea Basin, produced using GIA modelling (Shennan et al., 2018; Vink et al., 2007).

Past GIA studies for the North Sea produced regional sea-level histories either using GIA-modelling runs primarily set up for the British Isles (Clark et al., 2022; Shennan et al., 2000, 2018; Sturt et al., 2013; Bradley et al., 2011; Bradley, 2011; Ward et al., 2006; Lambeck, 1993, 1995), or ones set up primarily for south Scandinavia (Steffen and Wu, 2011; Vink et al., 2007; Steffen et al., 2006; Steffen and Kaufmann,

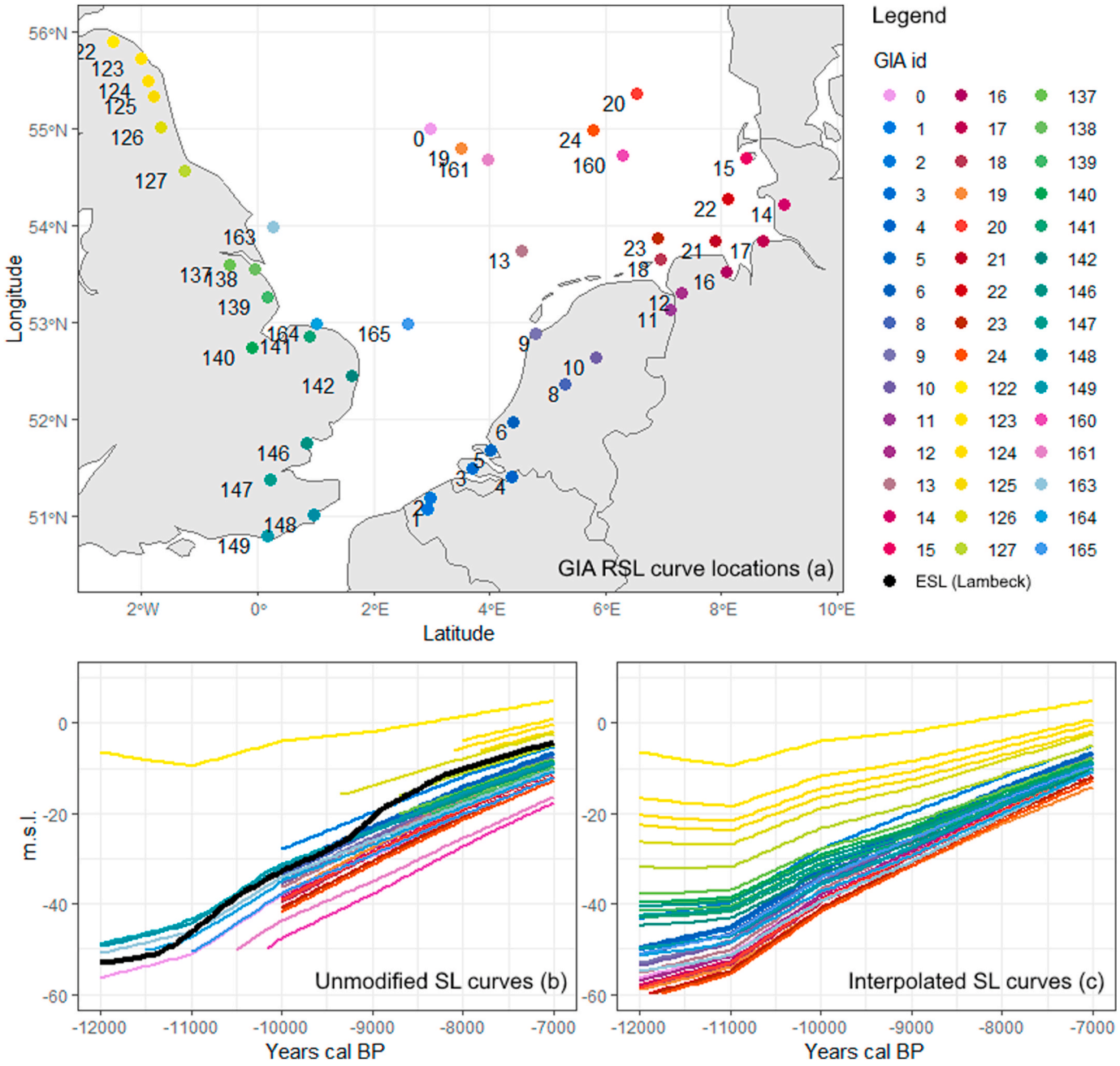

Fig. 4. a) GIA RSL curve locations from Kuchar et al., (2012): 0, Vink et al., (2007): 1–24, and Shennan et al., (2018): 122–165. b) age-depth plot for unmodified RSL and ESL curves, c) Interpolated RSL curves which are the basis for sea level surfaces (Fig. 5, see SI-3). GIA RSL error band is ±0.5 m overall, with higher uncertainty for the German coastal area at ±1 m during the Early Holocene (Vink et al., 2007: 3267).

2005; Peltier, 2002). The former do fairly well for the west of the study area, as their settings were optimised to fit British coastal and near-offshore geological data. The latter perform fairly well for the east of the study area. The central North Sea, however, is hardly tuneable owing to geological data quantity and quality limitations: Concurrent GIA models have produced deviating relative sea-level histories (Vermeersen et al., 2018; Cohen et al., 2017: 161-62). Though we await improvements in new generations of GIA modelling output that performs equally well across all sectors of the North Sea, we work with the currently best available models. We manually extracted the published relative sea-level reconstructions (RSL curves; Fig. 4) for the west-side and east-side North Sea (Shennan et al., 2018; Vink et al., 2007), confronted them with published geological data and blended this in into timestep-specific relative sea-level surfaces (SLS; Fig. 5). The RSL curves were extracted per 250-year timestep, resulting in synthetic point data with the relative sea level for each timestep for a series of locations.

As mentioned above, GIA-modelling derived sea-level histories are to match those gauged with geological sea-level indication points (SLIPs). For the North Sea basin, a large number of SLIPs has been collected over the past decades (Bungenstock et al., 2022; Hijma and Cohen, 2019; Meijles et al., 2018; Shennan et al., 2018; Vermeersen et al., 2018; Vink et al., 2007), and further efforts to synchronise datasets collected by different research groups are underway. The SLS blended sea-level history was created starting from selected RSL curves from Shennan et al. (2018; British side) and Vink et al. (2007; German Bight), together providing reasonable coverage of the southern North Sea (Fig. 4a). In the central North Sea, we nudged and deselected mis-fitting curves (Fig. 4, ids 160 and 161; see SI-3) based on Kuchar et al. (2012, see Fig. 4 id 0), because of the better fit for the Doggerbank (Emery et al., 2019: 13), and matched the curves to SLIP-based sea-level reconstructions findings of Hijma and Cohen (2019) and Meijles et al. (2018), consulting with Holocene sea-level research colleagues in the process (M. Hijma; K. de Wit). We note that typical North Sea SLIPs for 9-8 ka have uncertainties of ca. 1 m (adopting assessment in Vink et al., 2007: 3267) and regional GIA-modelling in the Early Holocene (before 8 ka) is considered to perform well when misfits of predictions to SLIP data are within 5 m (Bradley et al., 2011; Bradley, 2011). For the Middle Holocene the SLIPs have decimetre accuracy, concurrent GIA modelling is more convergent with misfits dropping within a meter.

Reporting of GIA RSL curves for single sites often cuts off display for time periods 'well prior to transgression' (Fig. 4b). For our modelling purpose, having them continuous was important. The blending of the SLS sea-level history thus also included extrapolation back in time (Fig. 4a). The extrapolations were based on the growth rates of each individual curve, and mimicked the development of curves that covered larger sections of the timeframe (Fig. 4 id's: 0 Doggerbank, 122 SE Scotland, 148 Essex, 149 Sussex, 163 Offshore Yorkshire, 164 NE Norfolk, and 165 Offshore Norfolk; See also SI-3). We then constructed raster grids for consecutive timeframes, interpolating the values read from Fig. 4b, and producing SLS covering the southern North Sea to be used to intersect (paleo)DEMs (Fig. 5). Using the 250y timesteps over the time frame 12-7 ka, resulted in 21 SLSs (see SI-1.2). The interpolation method used was SAGA's Thin Plate Spline, which is suitable for interpolating data with irregularly spaced points, creating smooth surfaces with flexible bending characteristics. Alternatives were deemed less suitable; for example Thin Plate Spline Triangulated Irregular Network (TIN) led to artefacts in areas with sparse data and steep changes, while B-Spline and Cubic Spline Approximation smoothed details and steep transitions too much for our needs.

3.1.3. *Corrections*

Non-GIA vertical land motion occurs in the North Sea Basin around the Central Graben due to basin background subsidence (BBS) and sediment loading (Cohen et al., 2022: 2905; Vink et al., 2007: 3259). This was described by Kooi et al. (1998), reporting background subsidence of 0.1–0.2 m/kyr, with higher values towards Dutch offshore locations closer to depocenters. Recent revision of base Quaternary mapping and expansion of this work towards the German Bight has resulted in updated BBS rates, locally changing values by ±0.03 m/kyr (Cohen et al., 2022: 2905-08), with a total maximum of 0.23 m/kyr in the research area (Fig. 6). Uncertainty is ±0.01/kyr for sites along the basin margin, and up to ±0.04/kyr in the offshore depocenters (*ibid.*).

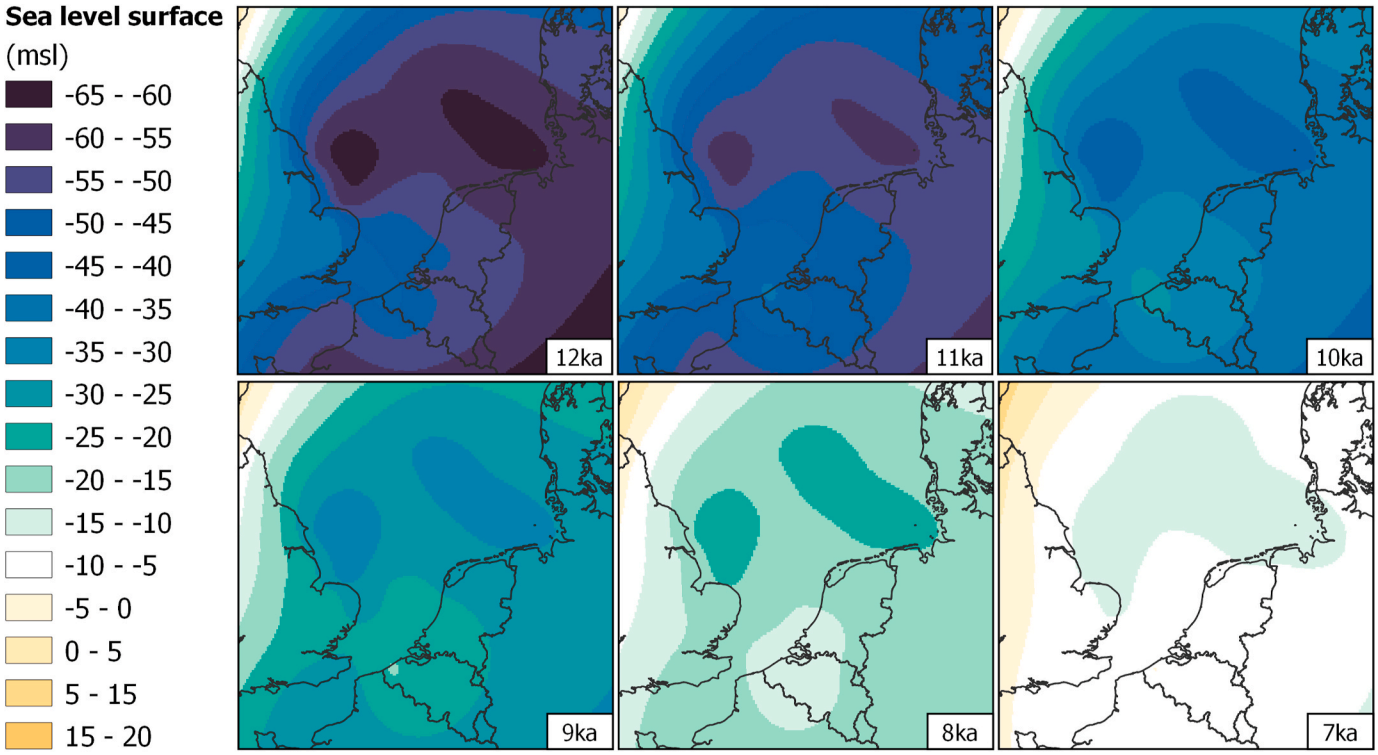

Fig. 5. Selection of millennial SLS output at 12-7 ka. Result of Thin Plate Spline interpolation (SAGA) of the finalised RSL curves (Fig. 4c).

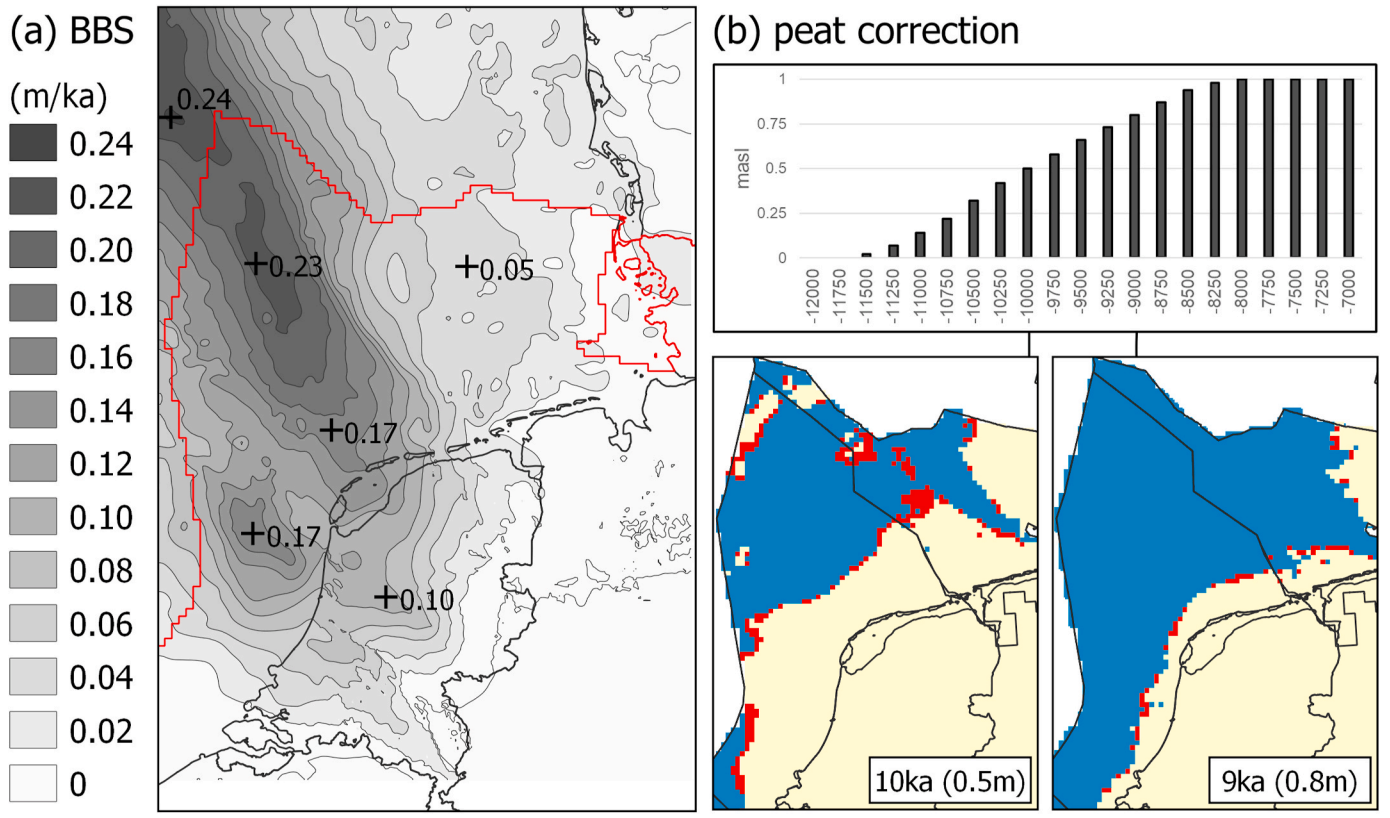

Fig. 6. a) Correction raster for tectonic background subsidence in the North Sea Basin (BBS), b) coastal peat growth elevation correction vector and the effect on lateral coastline positioning at 10 and 9 ka. BBS uncertainties are on the lower end in the coastal/near shore areas, i.e. 0.14 at 7 ka and 0.25 at 12 ka; and on the higher end further offshore near the depocenters, i.e. 0.3 at 7 ka and 0.5 at 12 ka (Cohen et al., 2022: 2905-08). Peat decompaction uncertainty is 0.2 for the thicker and younger onshore peat layers, and 0.1 for thinner and older offshore peat (Hijma and Cohen, 2019: 74).

Correcting for non-GIA background subsidence projects the paleoDEM surface in the eastern Doggerbank and northern Oyster Grounds, to positions ca. 2.75 ± 0.5 m higher at 12 ka than current encounter depth. Areas north and west of Holland project to ca. 2 ± 0.25 m higher at this time. At 7 ka, the offset decreases to ca. 1.6 ± 0.3 and 1.2 ± 0.15 m respectively.

Another correction concerns the nature of SLIP datasets used to gauge GIA models. Due to lateral groundwater flow, capillary effects, paludification occurs ahead of inundation, resulting in peat growth. This growth then leads to an elevation change in the coastal areas which would need to be corrected for in inundation modelling. Assessments of basal peat thickness and bulk density (feeding decompaction factors deployed in SLIP specifications; e.g. Hijma and Cohen, 2019: 74) show that pre-compaction near-coastal peat layers were up to 0.5 ± 0.1 m thick at 10 ka and up to 1.0 ± 0.2 m thick at 8 ka. Early Holocene peat beds encountered at depth offshore are typically around 0.16 m thick (covariant with the rapid transgression rates affecting this area). Here, a decompaction factor of 3 is considered. Bed thickness for Early to Middle Holocene peat encountered at depth below coastal plains (slower transgressed than the far offshore) is typically 0.4 m where overlain non-erosively by mud. For the former, a decompaction factor of 3 is considered and a factor of 2.5 for the latter (Hijma and Cohen, 2019: their SI). In both cases, the decompaction uncertainty is half the observed peat thickness. This decompaction is accounted for in the model by adding the correction value to the DEM before subtracting the SLS for coastline determination (see 3.1 section introduction). Fig. 6b shows the effect of including coastal peat elevation in inundation modelling, with red areas included as land if the correction is applied. In areas with a gradual coastal slope, seemingly small vertical corrections can lead to significant lateral coastline positioning difference.

3.1.4. *Model uncertainty*

Model output uncertainty comprises the error margins of the correction components and relative sea level rise outlined above. DEMs are upscaled to 5 × 5 km, giving a mean value for a large area, which leads to much lower uncertainty than for local palaeoelevation. Moreover, different DEMs are compared in the results (Bathymetry: IM0xx, paleoDEM: IM1xx and corrected paleoDEM: IM1x1 & IM1x2), so we do not consider an error margin for the DEM. Relative sea level uncertainty is ca. 5 m over the period 12-7 ka cal BP (e.g. Lambeck, 2014), this means the uncertainty per timestep is ±1.1 m ($\sqrt{(5^2/21)}$). For background subsidence, we consider higher uncertainties near the depocenters (±0.3 to ±0.5) than the basin margins (±0.15 to ±0.25), and for peat compaction higher uncertainty for younger, thicker layers (±0.2) than older, thinner layers (±0.1). Together, the square root of the sum of the squared uncertainties ($\sqrt{(RSL^2_{uncertainty} + BBS^2_{uncertainty} + PC_{uncertainty}{}^2)}$) gives a low model uncertainty of ±1.13 at the basin margins, and higher uncertainty in the depocenter of ±1.16 at 7 ka and ±1.21 at 12 ka. This vertical uncertainty does not exceed the tidal (T) and coastal peat (P) ribbons at 2 m below and above the estimated coastline (see 3.1 section introduction), nor the rate of sea level rise per timestep, which varies between 1.7 and 2.6 m per 250 years for the eastern region. Therefore, the T and P ribbons and the timesteps can be viewed as a conservative margin of error for coastline positioning and temporal patterns.

3.2. *Archaeological dates-as-data approaches*

Dates-as-data approaches take large datasets of archaeological radiocarbon dates as a proxy for past changes in human activity. They rely on the line of assumptions that a correlation exists between population density and the amount of occupation remains, the latter

influencing discovery chance, research interest and the number of radiocarbon dates. This relationship between data and past activity is of course much more complex, as taphonomic, research, and methodological biases are spatiotemporally differentiated and obscure and distort the archaeological record (Crema, 2022; Crema and Bevan, 2021, Larcombe and Ward, 2021; Perreault, 2019: 40–111). Critical reviews of these approaches discuss how spatiotemporal distribution of radiocarbon dates is affected by the accessibility and archaeological visibility of sites, preservation conditions, and the focus of research institutions and funds available to submit samples for dating (Carleton and Groucutt, 2021; Ward and Larcombe, 2021; Becerra-Valdivia et al., 2020; Attenbrow and Hiscock, 2015; Torfing, 2015). Visibility and preservation are key, and as some activities leave physical residues that are much more visible and likely to preserve than others (Perreault, 2019: 82–83), we think summed radiocarbon data can approximate changes in past activity at best; its relationship to population is more complicated (Hoebe et al., 2023a: 3). However, dates-as-data approaches continue to develop (Crema, 2022; Carleton and Groucutt, 2021; Williams, 2012), with new and improved methods geared towards dealing with the limitations of research bias (Timpson et al., 2014), taphonomic bias (Contreras and Codding, 2023; Bluhm and Surovell, 2019), and the influence of the calibration curve on the representation of summed radiocarbon data (Heaton, 2022; Price et al., 2021; Bronk Ramsey, 2017; Brown, 2017).

Although the limitations of these methods make their application controversial, there is also widespread recognition for their high potential. Studies employing dates-as-data approaches promise insight into large spatiotemporal patterns of changes within past societies (Lawrence et al., 2021; Palmisano et al., 2021), and in relation to external pressures such as sea-level rise, climate change and ecological hazards (Hoebe et al., 2023a; Mithen and Wicks, 2021; Van Maldegem et al., 2021; Crombé and Robinson, 2017; Waddington and Wicks, 2017; Robinson et al., 2013). Inundation modelling is valuable here because it provides information on the potential timing and extent of these external pressures as well as a general landscape history to contextualise the archaeological data. Moreover, components of the inundation model provide information about the sedimentary record and landscape taphonomy (Contreras and Codding, 2023; Ward and Larcombe, 2021), both of which are spatially differentiated and important confounding factors regarding the representativeness of the archaeological radiocarbon record (Hoebe et al., 2023a; Perreault, 2019: 83–85). Such data can contribute to identifying the spatiotemporal differences in accessibility and taphonomic bias affecting the archaeological record, and possibly provide ways forward in the correction of such biasing factors (see 5.2).

3.2.1. The dataset

The archaeological radiocarbon dataset we use to explore the relationship between inundation of the North Sea Basin and hunter-gatherer activity in NW Europe has been assembled from various sources (see SI-4.1), and has been extensively analysed and discussed (Hoebe et al. 2023a, 2023b; Vermeersch, 2023). The dataset presented in Hoebe et al. (2023a: 3–4) was expanded with new published datasets (Bird et al., 2022; Van der Plicht and Kuitems, 2022), further curated, and limited to the current research area (England, Belgium, the Netherlands and Niedersachsen). The dataset includes 3231 radiocarbon dates from 847 sites (SI-4.1). As in all large radiocarbon datasets, there are several inherent issues, such as differences in preservation, sampling strategy and research focus between geographic regions (Hoebe et al., 2023a: 9–13). Despite this, the overall pattern of activity density fluctuation survives stringent vetting procedures and correlates significantly with independently identified (regional) cultural changes, changing climate conditions and phases of sea-level rise (Hoebe et al. 2023a, 2023b). In this paper we take steps to further our understanding of patterns related to sea-level rise, cultural changes and taphonomy by contextualising spatial approaches to radiocarbon density fluctuations (Crema et al., 2017) with the landscape history provided by inundation modelling. To this end we provide results from regional composite kernel density estimates, rate of change, spatial permutation tests and mark permutation tests (see SI-4 and below). Radiocarbon date processing and analysis was done with the R package 'rcarbon' (Crema and Bevan, 2021).

3.2.2. Dates-as-data methods

In dates-as-data approaches, Sum Probability Densities or SPDs (Crema, 2022; Crema and Bevan, 2021) of large sets of calibrated radiocarbon dates are used; our dataset was calibrated with 'rcarbon' using Intcal20 (Reimer et al., 2020). Calibration curve patterns are amplified by summation, which makes fluctuations in SPDs impossible to interpret without model testing (ibid). This is especially true when normalisation is applied in the summation or calibration process, which results in peaks at steep sections of the calibration curve (Weninger et al., 2015). Composite Kernel Density Estimates or CKDEs more reliably reflect underlying patterns in the data (Bronk Ramsey, 2017; Brown, 2017). With this method, a randomly sampled calendar date is taken from each calibrated date's probability distribution. Kernel density estimates are generated with a user-defined bandwidth (50 years to allow the visualisation of generational-scale changes) and summed resulting in a curve similar to SPD. This process is repeated a number of times (500 simulations) and visualised as an envelope to account for calibration uncertainty (ibid; see SI-4.2).

As an exploratory tool we also apply Mark Permutation testing to SPDs of subsets of our dataset. Mark Permutation Testing allows for the formal comparison of the summed probability distribution of a radiocarbon dataset's subsets against the whole dataset (Crema, 2022; Crema and Bevan, 2021). This is done by assigning each date to a category and then aggregating these category-specific SPDs. The category labels assigned to the dates are then shuffled, which is repeated n (500) times, resulting in an envelope. Subset SPDs can be compared to see during which periods they differ significantly from the overall distribution. We use this to compare the density fluctuation of archaeology at a certain height above relative sea level in the eastern part of the dataset, provided by inundation model output. Height above RSL for each timestep was obtained from the IM for each site location in QGIS. Dates from those sites were then matched with the correct height above RSL for their corresponding timestep in R (see SI). Dates were then grouped according to elevation category (i.e. 0-50 m above RSL, more than 50 m above RSL), so that SPD fluctuation could be compared between landscape zones in relation to past sea level.

The method above provides insight into SPD fluctuations for larger, predefined regions in the research area. Insight into more localised differences in activity density, and patterns of growth and decline is essential to understand the impact of inundations. Spatial permutation testing (Crema et al., 2017) allows for this, which is a method that also relies on SPD. First, a growth rate null model is generated, calculating the rate of change in SPD density between defined (250y) timesteps (Brown, 2017). Locally weighted SPDs are generated, giving the probability density at a given location (weighted by the probability of contemporaneous neighbouring sites) at a given timestep. The permutation algorithm then shuffles the sites associated with each local SPD, which is repeated a number of times resulting in an observed local growth rate and a set of simulated growth rates for each location and at each timestep transition. Where observed local growth rates are significantly higher or lower than the simulated growth rate, this is indicated with a p value. Additionally, the spatial permutation test method includes correction for false discovery rate (Benjamini and Hochberg, 1995), computing q-values for locations that are less likely to be false positives. Whereas $p < 0.05$ implies that 5% of the results would be false positives, $q < 0.05$ implies that only 5% of the results with a q-value below 0.05 would be false positives (Crema et al., 2017: 4; see SI-4.2).

4. Results

4.1. Inundation models and the drowning of Doggerland

Eight inundation models (Table 2) were generated to compare the effects of different model components. The most basic inundation model (IM000) intersects a Bathymetric DEM with ESL. The correction effect that improvements upon this model have, is visualised in Fig. 7. Using a paleoDEM (IM100) over Bathymetry, or SLS over ESL (IM010) or applying BBS correction or not (IMxx1), each affects the IM000 model in spatially differential ways. The visualisation of the cumulative effect (Fig. 7d) explicates the improvement of IM111 over IM000.

The primary output of the inundation models are time-series maps, characterising the changing landscape across 21 timesteps between 12 and 7 ka cal BP. The full set of maps is given in the Supplementary Information, and a selection is given in Fig. 8, comparing the two highest quality models available for the eastern (IM112) and western (IM012) parts of the research area. As insufficient paleoDEM-construction data was available to us for the western North Sea, its effect on the model output can only be compared in the east.

4.1.1. General inundation model intercomparison

We performed a raster cell count for the inundated areas for all IM maps to calculate the difference in inundation in km^2 from one timestep to the next (Fig. 9) for the eastern part of the study area (Belgian-Dutch-German sectors). This overview makes the effects of different model components explicit in terms of the timing and area of inundation. Differences in the timing of inundation are driven mostly by the implementation of the SLS component. We highlight as main outcomes of IM intercomparison.

A) All SLS-driven IMs (IM01x and IM11x) show gradually increasing areal inundation rates starting after 11 ka. Inundation models based on ESL (IM000 and IM100), have considerable inundation occur before 11 ka, with a lowered rate around 10 ka. This difference is because the SLS corrects for GIA warping of the earth's crust (see Figs. 5 and 7b) which was higher during the Late Glacial and gradually lowered during the Early Holocene.

B) IMs implementing both SLS and paleoDEM (IM11x), are characterised by a very pronounced peak in the inundation rate at 10.25 ka of over 17,500 km^2 (ca 7000 km^2 per century). Irrespective of exact timing, we note that the these rapid areal inundation of the 11th millennium BP (11-10 ka) is caused by two factors: (1) strong RSL rise (e.g. Fig. 4) and (2) RSL rise passing a critical elevation zone where the study area hosts low-gradient terrain (between −50 and −40 m in (paleo)DEMs).

C) Relatively minor differences result from implementing the BBS correction (IM111) and adding the peat-thickness offset (IM112). It slightly decreases inundation in the timesteps leading up to the 10.25 ka peak and flattens the decreasing rate after 9.75 ka. Differences caused by the implementation of these corrections seem insignificant in terms of km^2 per timestep, but in the spatial output they are more pronounced (compare correction impact in Fig. 6 with Fig. 10; see also SI-5). Slight increases in the inundation rate early on in the timeseries lead to systematically earlier inundation of areas affected by tectonic subsidence, i.e. the eastern Dogger Bank and the eastern Oyster Grounds peninsula (compare Figs. 6 and 10).

Table 2
Inundation model codes (IM) and their components at different quality levels. The three numbers that constitute an IM code correspond to the quality levels of the DEM (1st), SL (2nd) and Correction (3rd number) applied in the model. ESL = eustatic sea level, SLS = sealevel surfaces; BBS = basin background subsidence, NA = no corrections applied.

IM	DEM		SL		Correction		
	0 BATHY	1 pDEM	0 ESL	1 SLS	0 NA	1 BBS	2 peat
IM000	X		x		x		
IM010	X			x	x		
IM011	x			x		x	
IM012	x			x		x	x
IM100		x	x		x		
IM110		x		x	x		
IM111		x		x		x	
IM112		x		x		x	x

4.1.2. Time-step specific inundation results

Below, the main changes over time are addressed based on the highest quality models for the east and west of the research area (IM012, IM112: Fig. 8), which compare the effect of using a paleoDEM over bathymetry on the timing and extent of inundation in the east, while both applying SLS and corrections. Coastline dating (Fig. 11) is compared with inundated areas (Fig. 12) between these two models (here visualised in 500y timesteps, though 250y output is available in SI-5).

4.1.2.1. 12th millennium BP: wetland formation in Doggerland. According to IM012 the North Doggerland coast extends from North Yorkshire north-eastwards to the Dogger Hills (terrestrial Doggerbank) and in the direction of Jutland (Fig. 11a). The Outer Silver Pit shows as a large paleolake situated between the Norfolk Banks and the Dogger Hills, west of the Oyster Ground lowlands. In the Southern Bight, there are extensive lowlands and wetlands where the rivers Thames, Rhine, Meuse and Scheldt would have converged between southeastern England and the western Netherlands and Flanders. The Elbe River system would have flowed through its lowland palaeovalley, which is seen as a well-defined feature in the IM112 output. Over the course of the 12th millennium, this palaeovalley transformed to estuary. Similarly, the IM112 output shows the eastern margins of the Outer Silver Pit paleolake to expand by about 11ka (earlier than modelled in IM012; Fig. 11a). The Outer Silver Pit transformed into a tidal inlet, opening the area up to Atlantic waters from the northwest (Fig. 8).

4.1.2.2. 11th millennium BP: inland seas and archipelago formation. During the first half of the millennium, the Elbe Palaeovalley inundates further, as well as the Oyster Grounds lowlands, which seem to become an inland sea, possibly with extensive tidal flats (Fig. 8). By the middle of the millennium, the eastern connection between the Dogger Hills and the North Frisian Peninsula (between the Oyster Grounds and Elbe Palaeovalley) is breached. By the end, after the extreme transgressions of this period, with ca. 15000 km^2 inundated in 250y (Fig. 12), Dogger Island and higher parts of the North Frisian Peninsula appear as an archipelago. The Southern Bight river-fed wetlands also expand further this millennium, transforming river mouths into estuaries and by the end developing into an inland sea (Fig. 8) with expansive tidal flats (at 10 ka in IM112; see e.g. Eisma et al., 1981). IM112 suggests an earlier timing of the separation of Britain from the mainland than IM012. Initially, the Southern Bight estuaries-fed embayment and the Outer Silver Pit tidal inlet system are separated by a 'land bridge' connecting Holland via the Norfolk Banks to Norfolk and its offshore. The likely paludified saddles of Norfolk Banks land bridge drown between 10.25 and 9.75 ka in IM112, compared to 9.5–9 ka in IM012 (Figs. 8 and 11, SI-5). We remark that younger Holocene sediment of tidal-marine origin is particularly thick (>5 m, locally up to 20 m) across the Norfolk Banks (Fig. 1) where our western (IM012) and eastern (IM112) areas join (Figs. 8, 11 and 12). Consequently the difference of a bathymetry-based DEM (IM012; late inundation) and geological-information tailored paleoDEM (IM112; early inundation) is particularly large. A conservative estimate of 5 m of Holocene sediment would already push back the IM012 inundation timing to 400 years earlier.

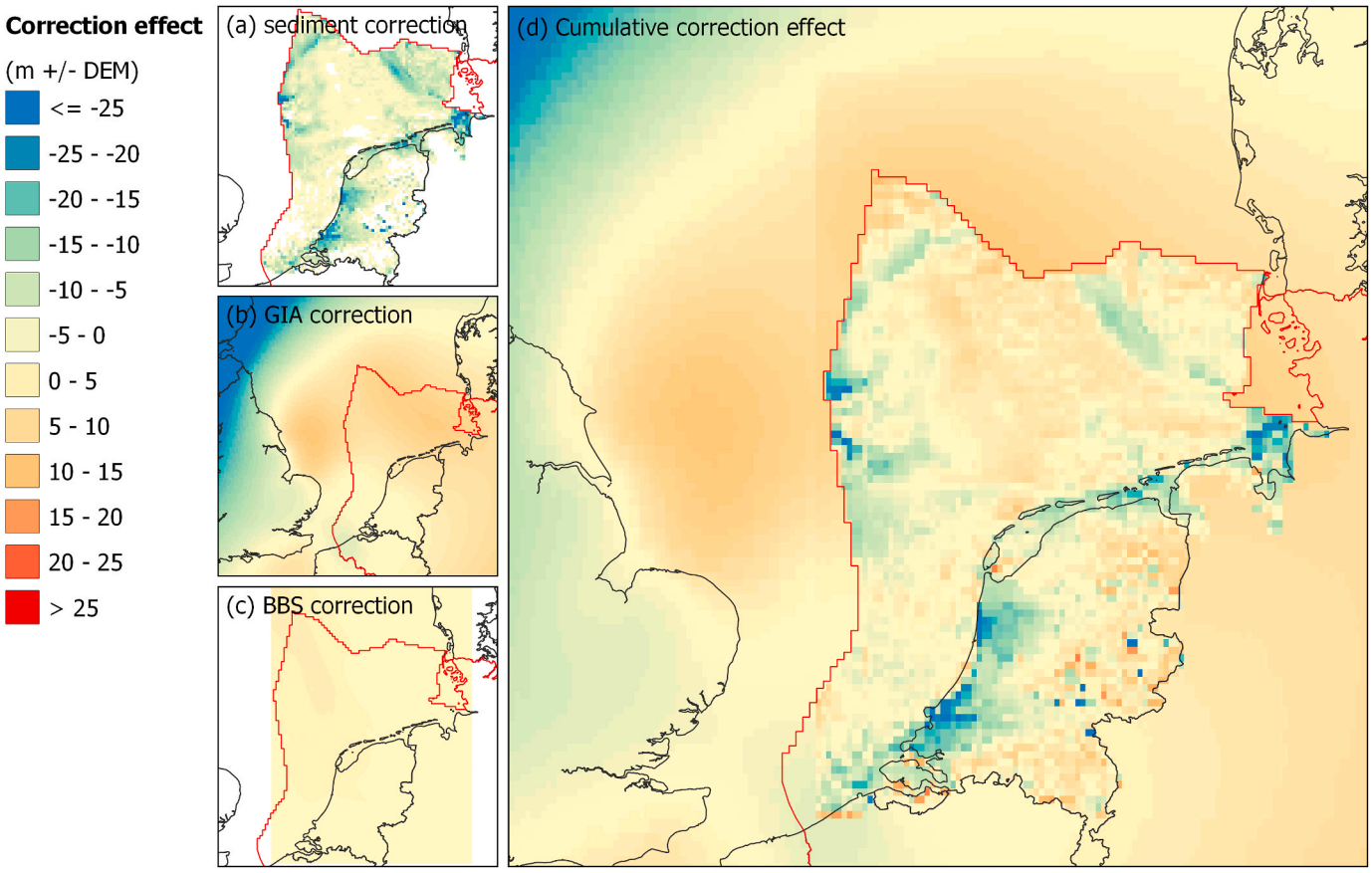

Fig. 7. The correction effect, i.e. the vertical impact of model components at ca.10ka in meters. This correction effect is given in relation to the IM000 model, consisting of Bathymetric DEM and ESL. The panels above visualise the effect of improving individual model components: (a) using a paleoDEM over Bathymetry, (b) using SLS over ESL, (c) correcting for BBS. These together have a cumulative, spatially differential effect (d).

4.1.2.3. 10th millennium BP: separation of Britain and drowning of the North Frisian Archipelago. At the start of the millennium in IM112 we see continued inundation causing loss of last connections by tidal flats between the Frisian mainland and the aforementioned North Frisian Archipelago and Dogger Island. Similarly, such tidal shoal connections form in the Norfolk Banks and disintegrate halfway the millennium (when the IM012 model has the land bridge breached; see above). By 9.5 ka, the North Frisian Archipelago and large portions of eastern Dogger Island is gone. The eastern shores of the North Sea still have extensive tidal flats and coastal wetland, which continue to gradually migrate landward. The pace of coastal inundation over areas north and northwest of Holland appear to be quite stable, with relatively little transgression over the course of the 10th millennium.

4.1.2.4. 9th and 8th millennium BP: gradual transgression and disappearance of Dogger Island. Over the course of these two millennia (Early to Middle Holocene transition), continued gradual transgression is seen on the eastern North Sea shores. Details in the IM112 output identify major palaeovalleys (Rhine-Meuse and Rhine in Western Netherlands; Ems, Weser and Elbe in Northwestern Germany), which topography were pathways to the transgression, eventually reaching inshore of modern barrier coastline positions (Figs. 11 and 12). The inshore palaeovalley reaches by the end of the 9th millennium had transformed into estuaries. The barrier systems featured in modern coastline (Holland coast, Wadden Sea coast) are result of coastal progradation younger than 7 ka (i.e. DEM-paleoDEM difference; Fig. 7). IM012 output is relevant to trace the gradual disappearance of the last remnants of Dogger Island and the peninsula off North Norfolk in the western North Sea, despite the ambiguity of using a DEM instead of a paleoDEM. The persistence of some islands in the English North Sea, may well be overestimated by several centuries. due to inclusion of Holocene subaqueous landforms in the IM012 DEM.

4.2. Inundation models and archaeological radiocarbon data

Not withstanding complications of potential research- and taphonomic bias (addressed in section 5.2), systematically processed archaeological radiocarbon dates from around the North Sea (section 3.2) provides insight into the density of excavated Mesolithic hunter-gatherer sites, and potentially also into fluctuations in human activity or demography in relation to inundation. The overall probability density estimate for the research area (Fig. 13a) shows the same pattern as published earlier (Hoebe et al., 2023a), which discussed the potential impact of climate events on human activity. In the Composite Kernel Density estimates we observe a gradual increase from the start of the Holocene onwards reaching a peak around 9.75 ka (Fig. 13a). The probability density declines to a trough around 9.5 ka, and then again increases towards an 8.75 ka peak, followed by a steady decline towards 7.5 ka. As established in Hoebe et al. (2023a), summed probability declines with a delay following the 11.4 ka event (Preboreal oscillation) and following the 8.2 ka event. However, following the 10.3ka event and the 9.5 ka trough, summed probability rises and forms notable peaks during the Early and Late Boreal. These peaks were discussed as potentially related to inundations in Doggerland (Hoebe, 2023a; Crombé, 2019; referencing IM output of Sturt et al., 2013). The generally rising density after 7.5 ka is regarded due to research-bias (the Late Mesolithic having received particular attention in the Dutch wetland archaeology).

When split results for the western (Fig. 13b) and eastern parts

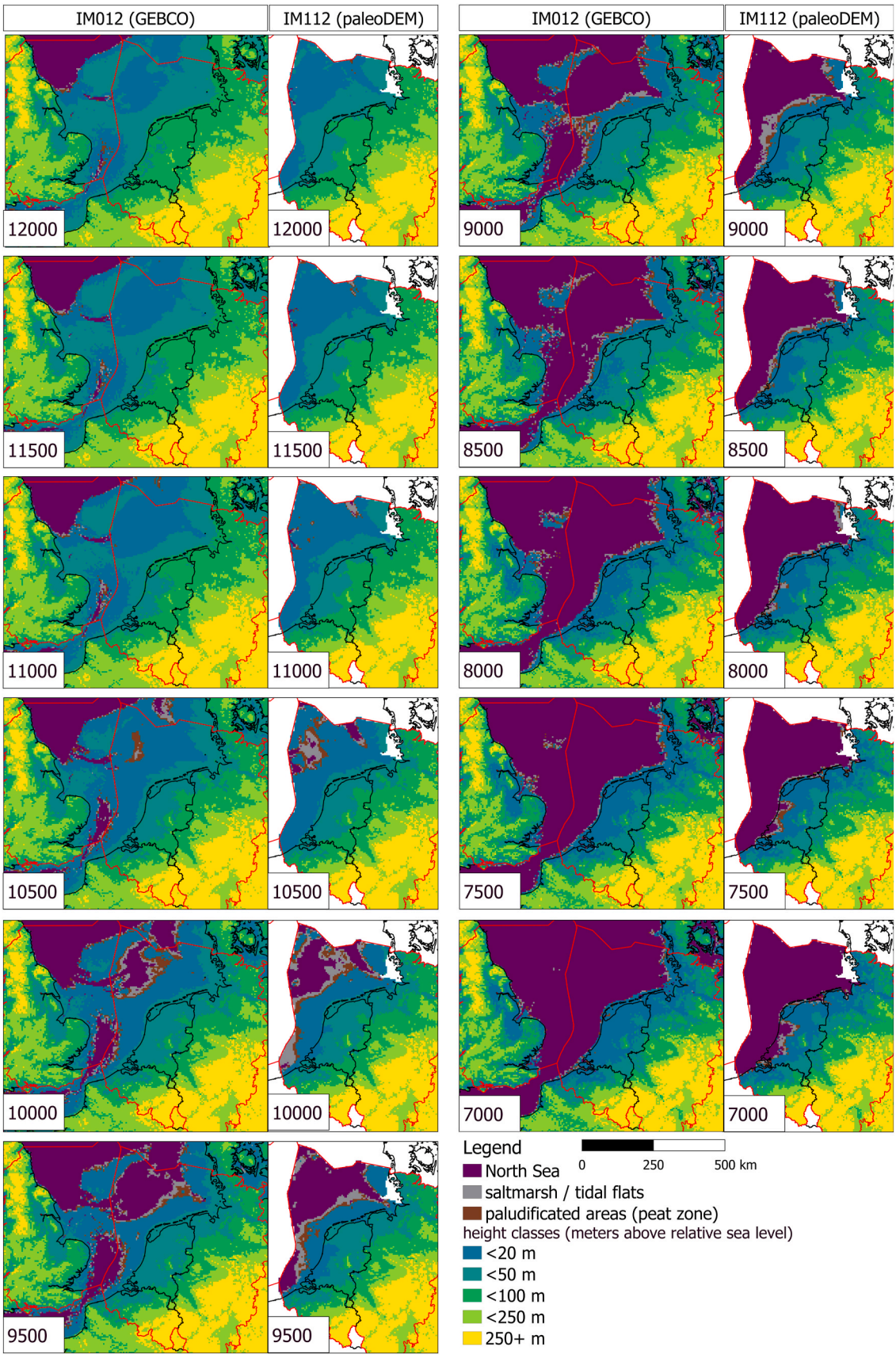

Fig. 8. palaeogeographic model outputs from 12-7ka in 500 y timesteps. For each timestep we provide a GEBCO based model (IM012) covering the entire research area and a paleoDEM based model (IM112) covering the Eastern section of the research area. Output at 250y timesteps are provided in the supplements (SI-5).

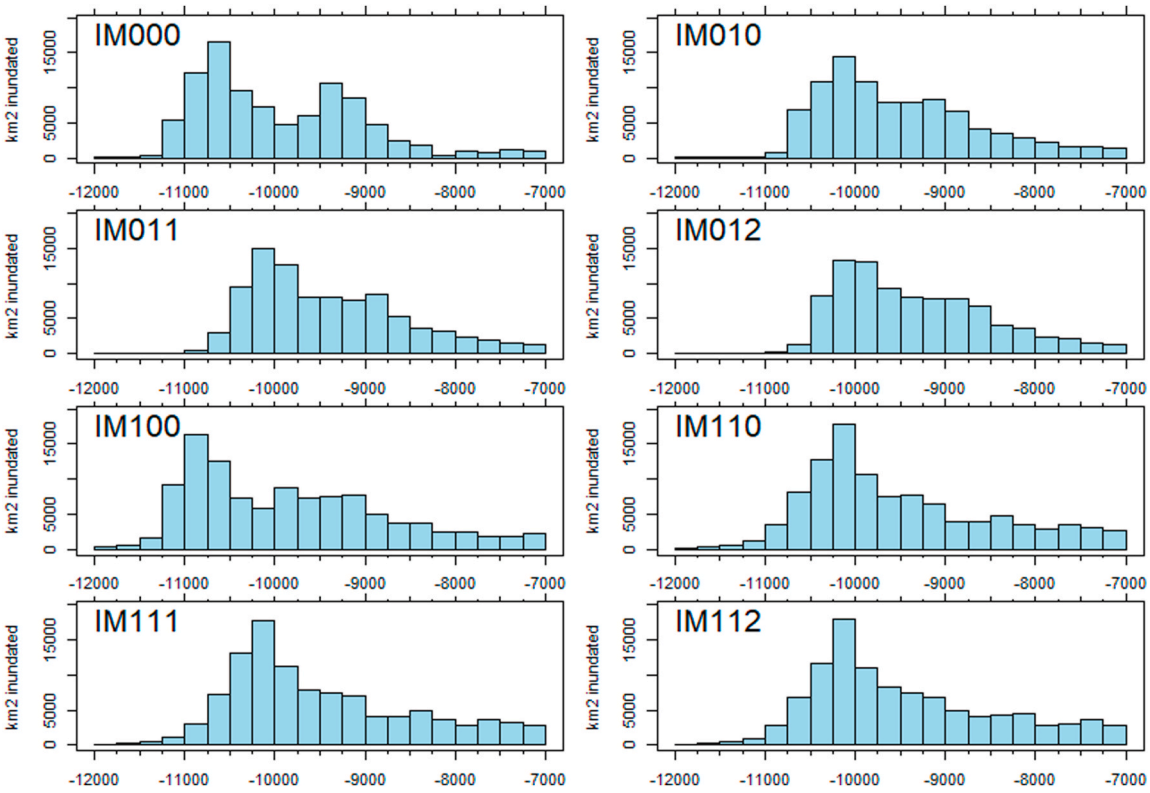

Fig. 9. Inundation model histogram output of area (km2) drowned per 250y timestep in the eastern part of the North Sea, for eight variants of the modelling. Key to IM naming provided in Fig. 2. IM000 is the least, IM112 the most sophisticated IM.

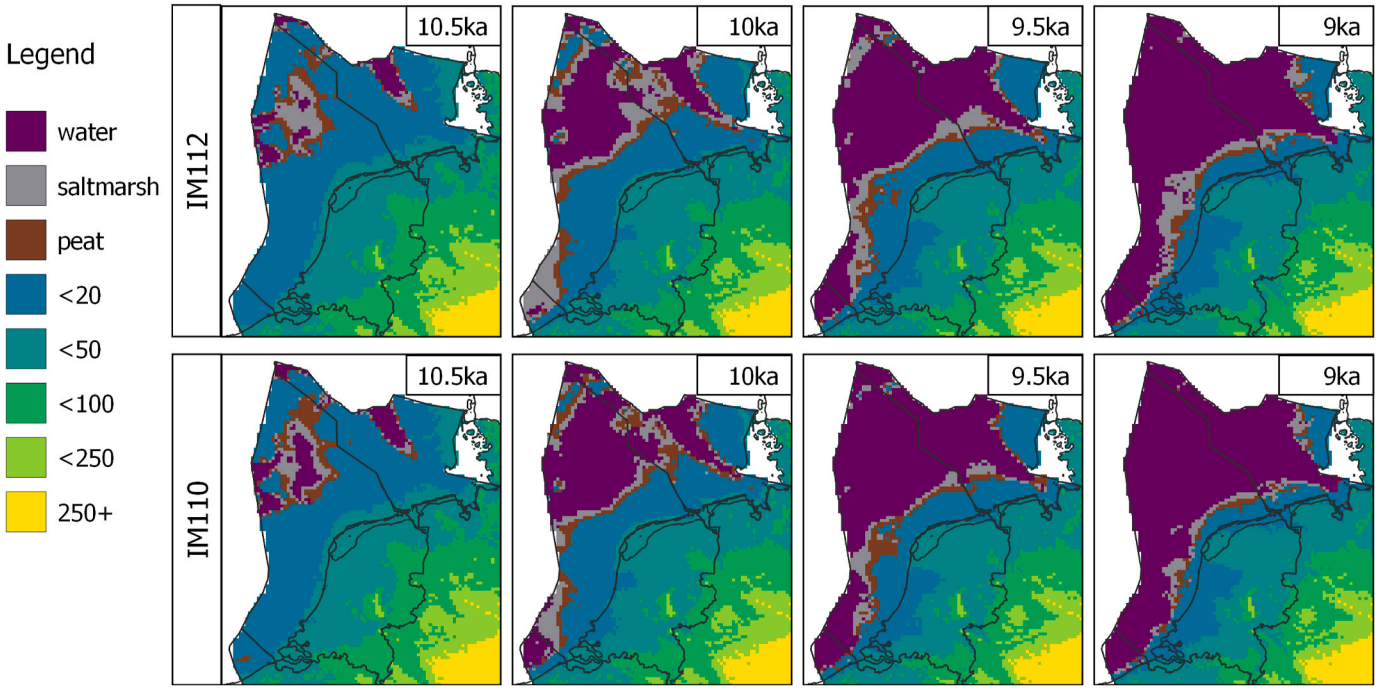

Fig. 10. Inundation model output for the eastern North Sea region, comparing the paleoDEM + SLS (IM11x) models without (IM112, above) and with (IM110, below) BBS and peat corrections at 10.5, 10, 9.5 and 9 ka.

(Fig. 13c) are compared, the latter (83% of the dates; 73% of the sites) echoes the overall result, with prominent peaks during the Boreal. For the west (Fig. 13b; 17% of the dates; 27% of the sites) we see relatively higher density in the Preboreal and Early Boreal than for the Late Boreal and Atlantic, which shows a pattern of gradual fluctuating decline. Lastly, the rate of change plot (Fig. 13d; see SI-4.2 for regional such plots) allows comparing growth rates in the archaeological dataset per 250-yr time steps. Within the Boreal, substantial fluctuations in rate of

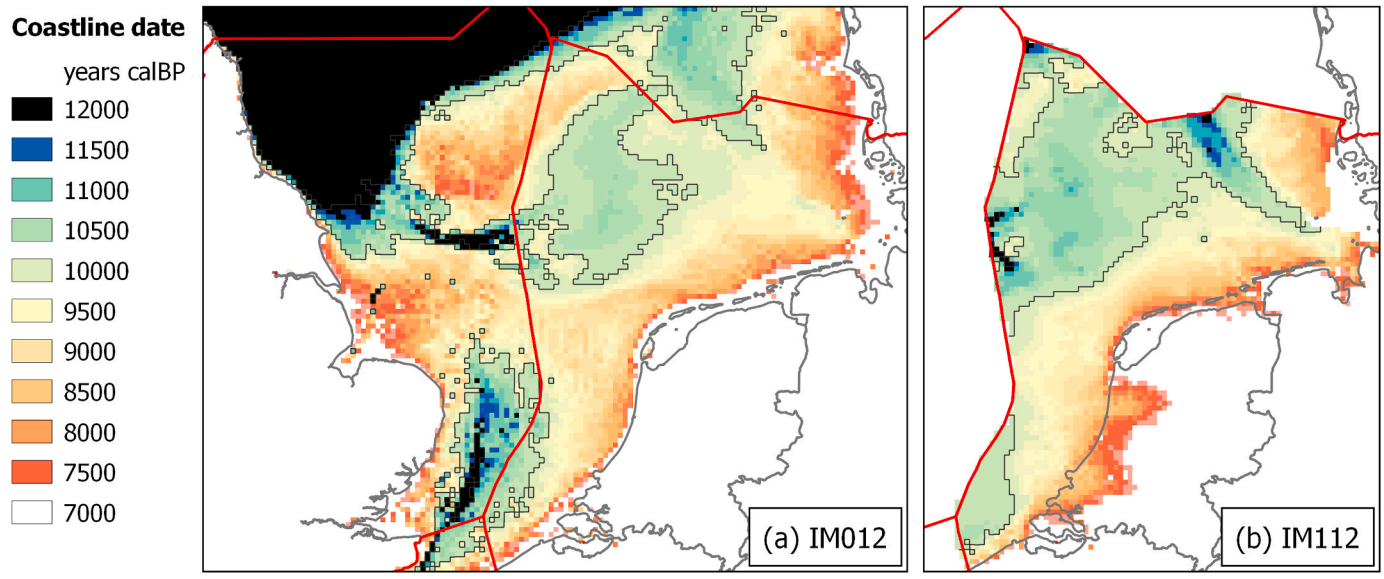

Fig. 11. Coastline dates for IM012 and IM112. Coastline at 10ka is outlined for reference. IM112 has earlier drowning of e.g. Elbe palaeovally, the connection to Britain, and the Dogger Bank.

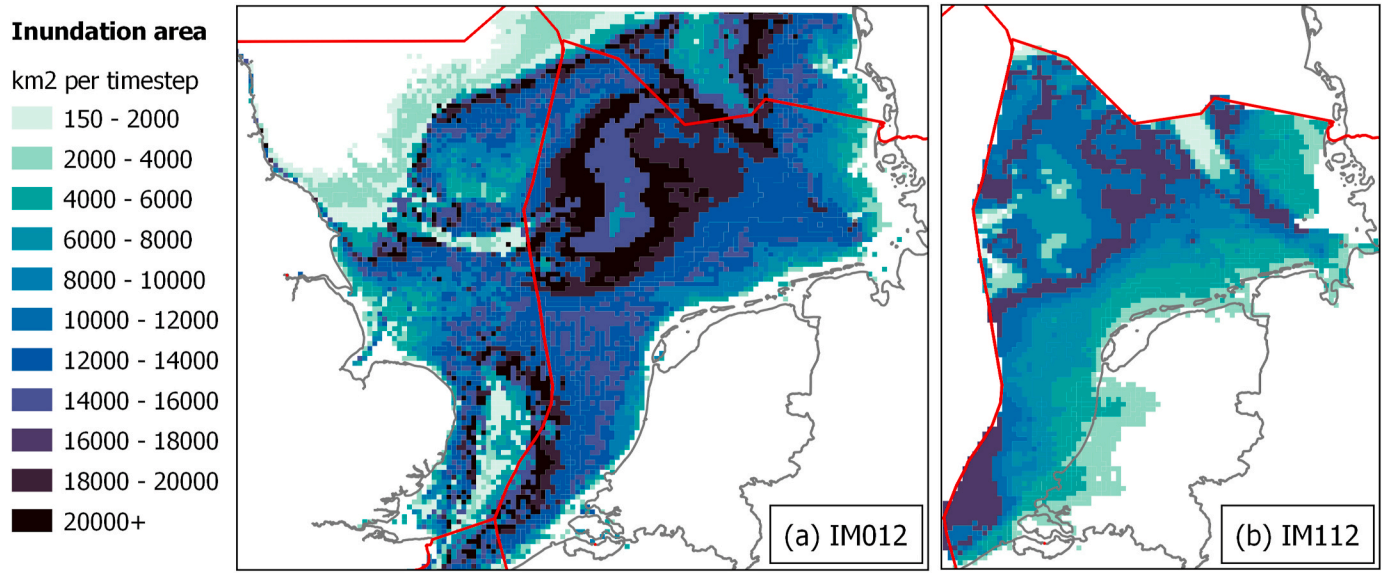

Fig. 12. Inundated area (km2) per 250y timestep for IM012 (east and west combined) and IM112 (east).

change occur around 10.3 ka and 9.3 ka, corresponding to climatic events and/or coeval inundation events as compounding risks.

Whether the overall trends in the growth rate hold across the study region was tested with spatial permutation tests (SPT; Crema, 2022; Crema et al., 2017), which were used to calculate the spatial heterogeneity in growth and decline in the dataset across the research area. SPT results (SI-4.2) showed significant local deviations in growth rate for four time periods around 10.5, 10.25, 9.25 ka and 7.75 ka (labelled I-IV; also indicated in Fig. 13b and c). Note that these local differences in growth rate may be related to changes in past human behaviour (demography, migration patterns), but will in large part be also shaped by dataset biases (accessibility, taphonomy, research history), addressed in Section 5.2.

In Fig. 14, the SPT results for these four time periods are visually compared to corresponding IM output (sections 3.1 and 4.1). Highlighted site locations show significantly higher or lower local growth than average. SPT identifies offshore North Sea finds as positive growth rate deviation in period I (10.75–10.5 to 10.5–10.25; ka Fig. 14a), i.e. in the centuries leading up to actual paludification and inundation of this part of the North Sea (10.25–9.75ka; Figs. 8 and 11b). SPT identifies positive growth rates deviations in Northern Netherlands and Northwest Germany for the time periods II, III and IV, mirrored by negative deviations in England (Fig. 14b–d). Dramatic land loss occurs off the Dutch and German mainland in eastern Doggerland during these timesteps, with ca. 30,000 km^2 of a land lost between 10.5 and 10 ka cal BP (Fig. 9), i.e. in time period II. At the same time, western England shows significantly lower-than-average growth rates (though growth rates are still positive). For time periods III and IV (from 9.5 to 9 ka respectively 8-7.5 ka), while Doggerland land loss continued, SPT continues to identify significantly different rates in the east (higher than average) and west (lower).

The inundation model output also allows the approximation of the relative height above sea level of archaeological sites. We compare the SPD of sites situated higher and lower than 50 masl with the overall

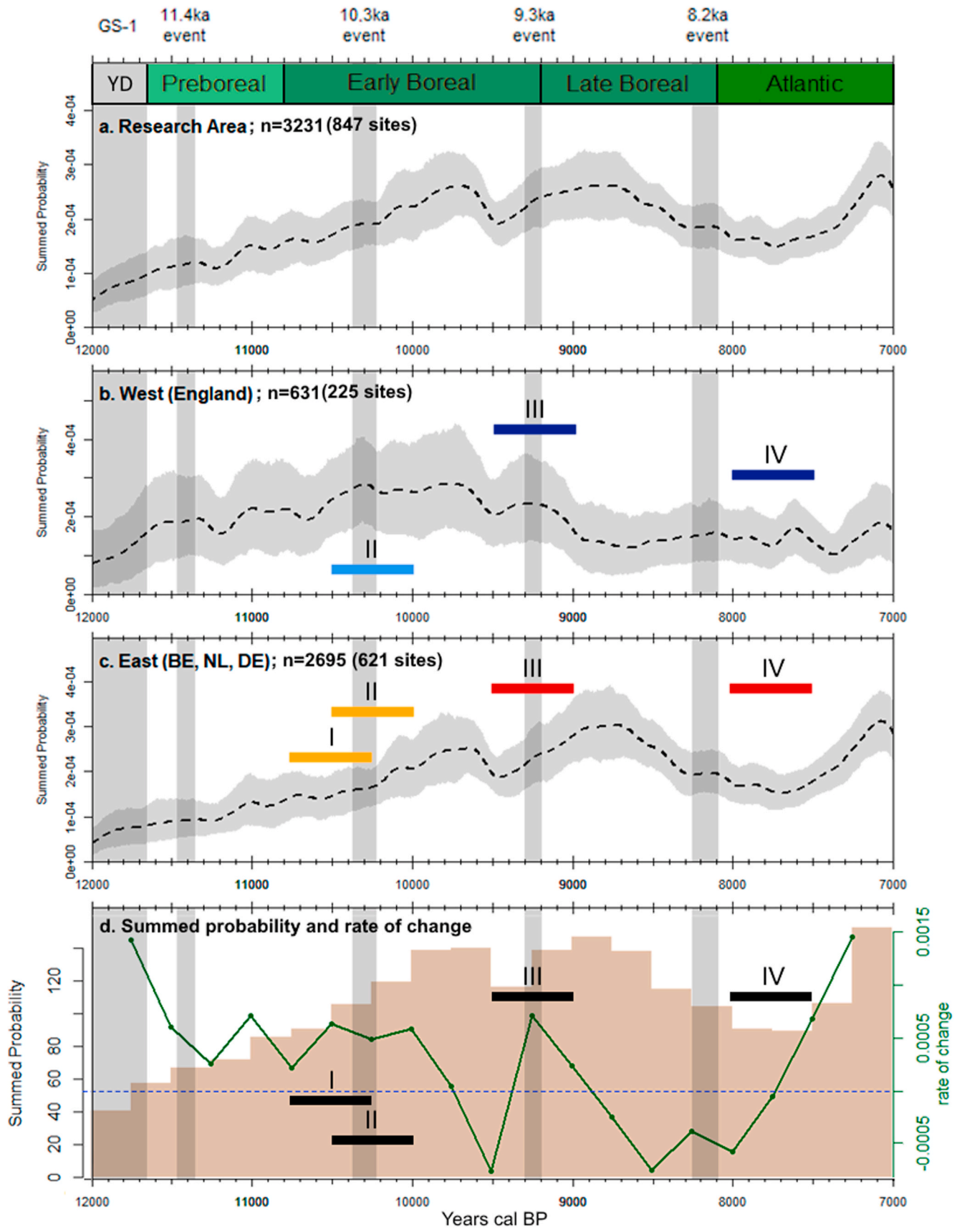

Fig. 13. Composite Kernel Density Estimates (see section 3.2.2) of the radiocarbon dataset for a) the entire research area, b) the western and c) eastern subsets; and d) summed probability histogram and rate of change. I – IV are selected time periods of significant subregional differences in growth rate, resulting from the Spatial Permutation Testing (Fig. 14).

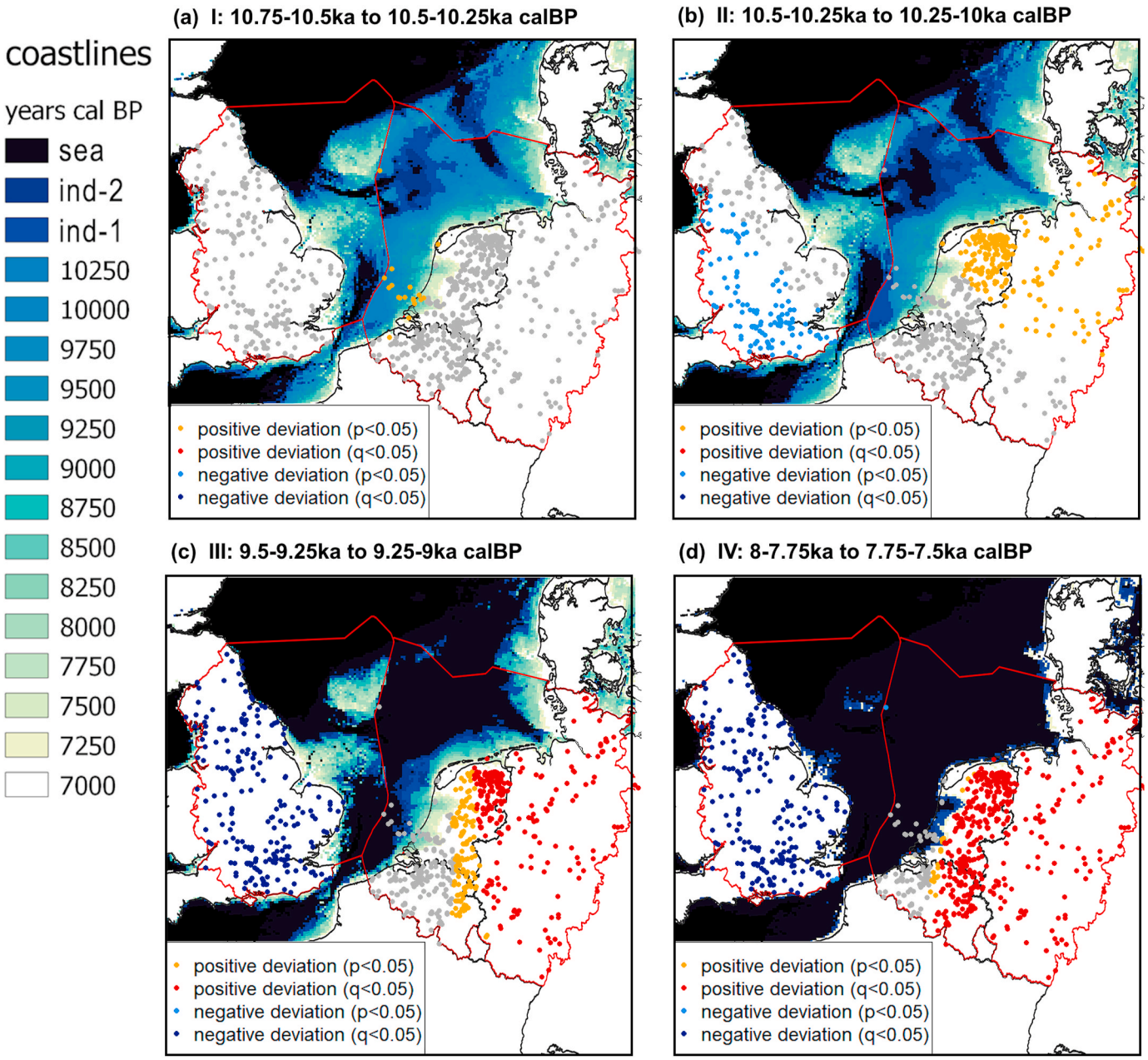

Fig. 14. Selection of significant Spatial Permutation Test (see section 3.2.2) results in relation to the temporally relevant inundation model output (west: IM012, east: IM112). The yellow to blue colour-scale signifies coastlines date (Fig. 11). In the four selected SPTs, areas inundated in the previous two timesteps were highlighted in deeper shades of blue (ind-2, ind-1). E.g. in timestep I (a, top left) the coastline of 10.25ka is visualised, and the areas inundated in the two previous time steps (10.75–10.25 ka BP) are highlighted in dark blue.

distribution using mark premutation test (Figs. 15 and 3.2.2). A distribution map is given at 10 ka as an example (Fig. 15a).The results show how the distribution of the lowland (<50 masl) and inland (≥50 masl) radiocarbon date subsets differ significantly from each other. In the eastern dataset (Fig. 15g and h), lowland sites older than 10 ka are hardly represented. Lowland site density increases following 10.25 ka (when inundation rates are particularly large; Fig. 15e and f), and becomes significantly more prominent than inland site density after ca 9.5 ka. This gives more insight into the timing and landscape context of the changes observed at time periods II and III in the spatial permutation tests (Fig. 14b and c) and the overall SPDs (Fig. 13a–c) ka. In the western dataset (Fig. 15c and d), we see the same overall pattern, though much less pronounced and with shorter significant deviations with smaller effect sizes (deviation from the overall pattern).

5. Discussion

5.1. Inundation modelled palaeogeography

Lateral inundation is driven by sea-level rise, but when expressed in rates of area lost is also highly dependent on the elevation and relief of the inundating landscapes. Improving paleo-elevation estimates at the time of marine transgression is essential for insight in the timing of transgressions and the extent of inundated and paludificated areas. Our comparison of inundation models made explicit how model components of different quality/accuracy levels impact outcomes (Figs. 9 and SI). Using paleoDEMs in inundation models better approximates the timing of key palaeogeographic changes in the region. Similarly, accounting for known processes such as basin background subsidence (Cohen et al.,

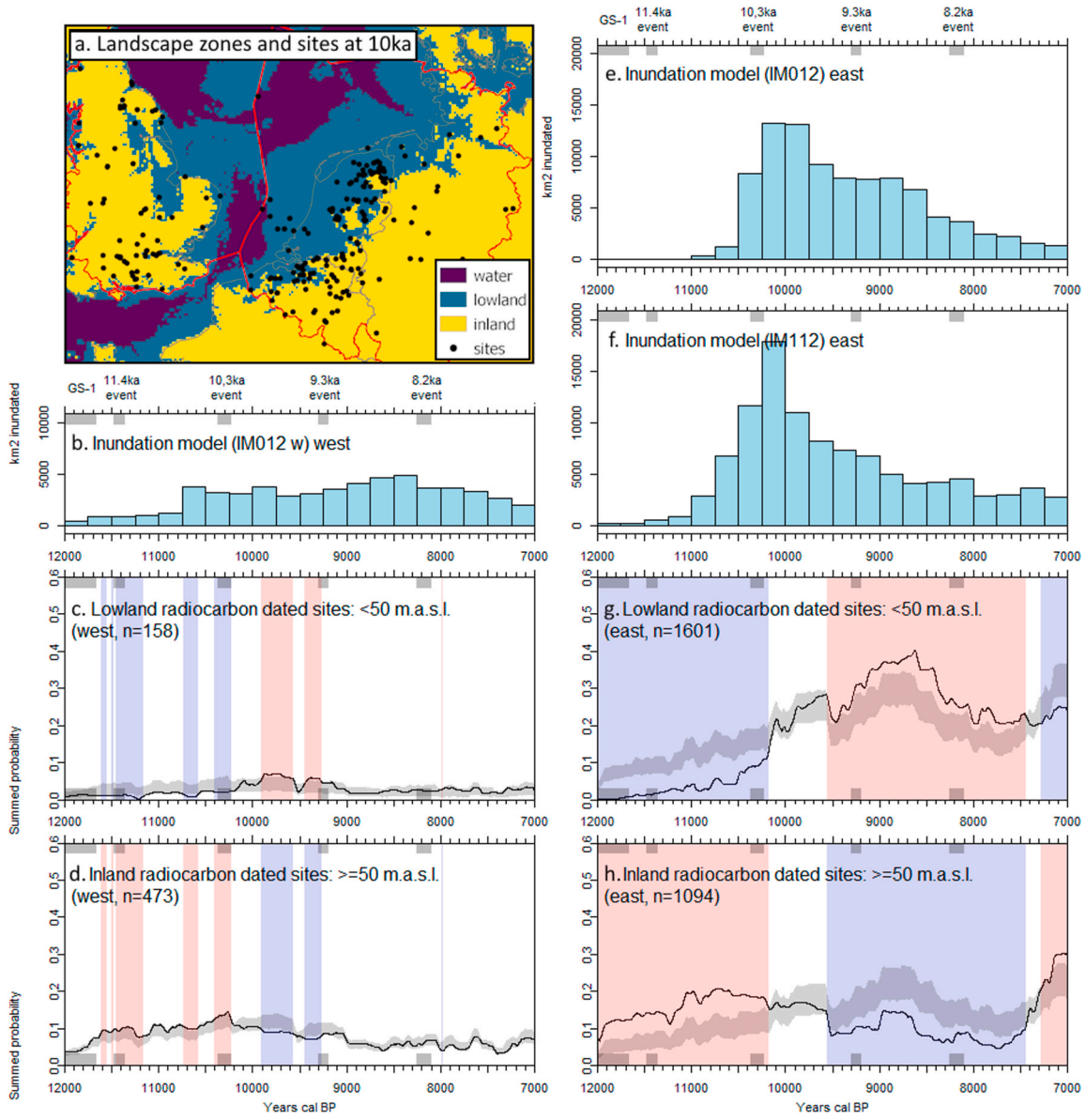

Fig. 15. Comparison of inundation models IM012 (W and E) and IM112 (East) with Permutation tests of the western and eastern part of the dataset. Example of the spatial distribution of coastal and inland regions at 10ka is given in the top left.

2022; Kooi et al., 1998) when confronting DEMs with GIA sea-level histories and factoring in coastal peat thickness in our models (Hijma and Cohen, 2019) necessarily improves the timing of inundation. While the effects of these corrections are small on the level of individual timesteps, they are cumulative over time and locally add up to meters of difference across the 12-7 ka timeframe. These corrections 'slow down' the rate of inundation in the model output.

Compared to IM112, earlier studies working with bathymetric elevation data in combination with GIA (the results of Sturt et al., 2013, Brooks et al., 2011, Van der Molen and De Swart, 2001; Lambeck, 1995 for example, each are IM010 equivalents), appear to have systematically underestimated the time of transgression in areas where large portions of the Late Pleistocene surface is covered with volumes of later sediment (inundate too late), and overestimate the timing for locations that saw later erosion. Initially, such choices may have been warranted because GIA data-model cross-validation revealed 5–10 m uncertainties for Early Holocene situations. This study showed that with improved GIA model resolution (e.g. Bradley et al., 2011; Steffen and Wu, 2011), improving DEM treatment in inundation modelling (Cohen et al., 2014) was indeed timely. Inundated area data (Fig. 9) shows that this adds up to a ca 8500 km^2 less inundated area in IM010 at 9.5 ka, and even 12500 km^2 at 7 ka. Global visualisations that use bathymetry with ESL on the other hand (IM000 equivalents), greatly overestimate the time of transgression (inundate too early) due to the effect of glacio-isostatic adjustment. In such models, an area of almost 23,000 km^2 more is inundated at 10.5 ka than in IM112, this difference drops towards later timesteps eventually leading to an underestimation of inundated area of ca 9500 km^2 at 7 ka.

Particular indications of our most developed model IM112 (see Figs. 8 and SI) can be extracted for mainland Europe land connections to Britain and to Dogger Bank. Concerning land connecting Britain, the critical area started dropping below sea level between 10 and 9.5 ka, and loss of low-tide mudflats in IM112 occurs ca. 9.25–9 ka. This chronology for breaching of this land bridge is > 500 years earlier than depicted in earlier IM studies (ca. 9-8.5ka; Sturt et al., 2013: 3970). Even later timings (8-7.5 ka Sturt et al., 2013: 3972; Brooks et al., 2011) have been discussed based on coastal peats along the south coast of England (Gupta et al., 2017; Massey et al., 2008). Separation between 9.25-8.75 ka is postulated by Behre (2007). Evidence for the mixing of southern and

northern sources of water in the Skaggerak was obtained from marine sediment indicators and dated at ca. 8.5 ka (Gyllencreutz, 2005; Streif, 2004). We suggest to favour IM112's 9.25–9 ka low-tide result as the true breaching and true marine connection. A low-tide connection may have persisted longer before water depths increased enough to allow for current systems to establish (Cohen et al., 2017: 163). Concerning connection to Dogger Bank, IM112 highlights that when this became an island (c. 10.5–10.25 ka), it appears connected to mainland Europe by smaller Islands and mud flats off the retreating North Frisian coast. Concerning the subsequent shrinking of Dogger Island, IM112 gives direct results only for its eastern 'tail', which steadily diminished between 10.25-9.75 ka, and becoming mostly intertidal by 9.5 ka, though small islands are suggested until 9-8.75 ka. This close to 1000 years earlier than previously modelled for this side of the island (9-8ka; Sturt et al., 2013: 3970). By ca. 8 ka, North Sea coastal areas were impacted by the so-called Storegga tsunami (e.g. Smith et al., 2004), for which local erosion, depositional and contained proxy information has been recently investigated (Nyland et al., 2021; Blankholm, 2020; Gaffney et al., 2020; Larcombe and Ward, 2018). We do not regard our IM112 or IM012 results to majorly change assessment of tsunami impact (depositional, taphonomical or archaeological) in southern parts of the North Sea, other than reducing the size of Dogger Island at time of impact. Full submergence of the Dogger Island is modelled at 8-7.5 ka (*ibid.*) and considers the western sector of the island (e.g. Fig. 15).

5.2. Interpreting archaeological patterns and landscape taphonomy

At the outset we identified two key ways in which better inundation models can improve the contextualisation of archaeology in this region. First, large- (spatiotemporal) scale studies of human behaviour and the way they relate to external pressures of climate- and environmental change clearly benefit from better insight into the timing, magnitude and spatial extent of inundations. Below we further address how inundation models can help improve hypothesis testing in dates-as-data approaches specifically. Second, new archaeological finds from the North Sea floor require contextualisation after dating and can benefit from placing them in a landscape context. Inundation models can provide this context, as well as a *terminus ante quem* (±250 years) for regions in the North Sea (see 3.1.4).

The dates-as-data approach methods result in several patterns that correlate to the timing of inundations. Some of these may relate to changes in human activity in response to sea-level rise, such as changing cultural practices, migrations and demographic change, and subsistence. However, several confounding factors complicate inference. The spatially differential impact of taphonomy on the mixing and loss of archaeological data, especially its accessibility and preservation, cannot be underestimated (Perreault, 2019: 40–111). Unravelling the impact of taphonomy on a radiocarbon dataset is complex, case-study specific and requires data on sedimentation, erosion and the preservation potential of sediments (Ward and Larcombe, 2021; Perreault, 2019). This is especially essential in the context of research areas with complex inundation history, such as the North Sea basin.

Taphonomic correction for dates-as-data approaches are beginning to be explored and improved. Previous studies have focused on general over-time changes in preservation potential (Surovell et al., 2009), and recently on the proportionality of landscape types and their preservation potential for archaeological data of a certain age (Contreras and Codding, 2023). While setting up a new method for taphonomic correction is outside the scope of this paper, we outline how paleoDEMs and inundation model results can improve future taphonomic correction efforts in dates-as-data approaches.

5.2.1. Accessibility and sedimentation

Holocene sediment thickness (Figs. 3 and 7) and coastline dating results (Fig. 11) provide important information about the accessibility of Mesolithic archaeological material. Comparing these results shows the age of coastal zones in the research area that are covered by significant Holocene sediments (Fig. 16). This is an indicator of potentially favourable preservation conditions of coastal contexts of specific age, but also of low accessibility (Perreault, 2019: 84–85). Excavated Early Mesolithic coastal contexts are rare, because of the history of inundation. They are preserved and accessible in areas affected by isostatic uplift or shallow seas. Such sites often contain well preserved midden layers owing to persistent re-use of locales that preserve information on subsistence practices and even burial (Bailey and Hardy, 2021; Milner et al., 2007). Fig. 16 can be seen as an indicator of how accessibility potentially influenced the representation of certain periods and regions in the dates-as-data results. This comparison shows that Holocene sediments mostly cover coastal areas dating to the end of the 11th millennium cal BP. This makes sense as sedimentation relates to transgression, and this period saw the most extensive phases of inundation (Fig. 9). However, a good portion of these coastal areas (ca 3500 km2) are only covered by 0–0.5m of sediment, making them relatively accessible, i.e. archaeological (and palaeontological) materials closer to the seafloor have a bigger chance of being detected or exposed e.g. by shallow disturbances or natural erosion. The overall lowered accessibility of lowland areas older than 10 ka is mirrored in the mark permutation test results (Fig. 15). Holocene sediment coverage on these contexts greatly reduced discovery chance of archaeological remains, and their representation in radiocarbon datasets.

5.2.2. Landscape zone proportion

The process of marine transgression during the Early Holocene not only transformed the character of landscape zones, but also affected their proportional representation within the research area. Over time, the proportion that represents archaeologically accessible coastal landscapes fluctuates. A larger proportion of available coastal contexts in the research area will date to the mid 11th millennium cal BP (Fig. 17). As the North Sea gains 'ground', the proportion of inland landscapes and associated archaeology will also decrease over time (Fig. 17). This has important implications for model testing in dates-as-data approaches. Given this change in proportionality, slightly increased radiocarbon data density in lowland landscapes around the 11th millennium cal BP, and a gradual decrease in inland landscapes, would actually reflect uniformity, rather than changes in human activity. If we expect higher density of human activity in coastal areas, this pattern of coastal proportionality would be amplified in dates-as-data frequency distributions.

Improved taphonomic correction of dates-as-data results (Contreras and Codding, 2023; Bluhm and Surovell, 2019; Surovell et al., 2009) should take research-area specific geoarchaeological data into account (Ward and Larcombe, 2021; Larcombe and Ward, 2018) such as accessibility and the changing proportions of inland and coastal landscapes in the research area. Other factors to be considered are erosion and preservation potential of different sediments (e.g. Kibblewhite et al., 2015). As older lowland and coastal zones are more often inundated or submerged, their potential for preserving Mesolithic organic remains is much higher than dryland archaeology.

5.2.3. Patterns and taphonomy

Seen in the light of temporal differences in taphonomy and accessibility, patterns of changing radiocarbon density reviewed in the results (4.2), can be further qualified. Periods of significantly deviating local growth rates were identified during the 11th millennium cal BP (Fig. 14a and b). The highlighted North Sea finds around 10.5 ka hail from a lowland area covered by little Holocene sediment (0–0.5 m) which saw gradual submergence over the course of the following millennium. Moreover, their discovery is owed to specific present-day offshore activities such as sand extraction and trawling (Peeters and Amkreutz, 2020; Amkreutz et al., 2018). The second period with significant local growth rate deviations (around 10.25 ka Fig. 14b) highlights elevated growth rates in the northwest of Germany and the Netherlands. A large

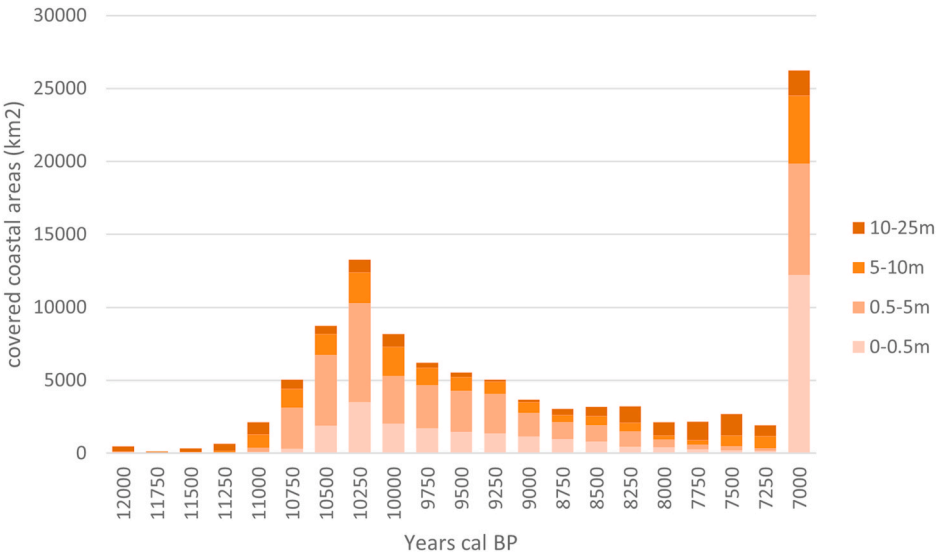

Fig. 16. The coverage of dated coastal areas (IM112, Fig. 11) beneath Holocene sediments of different thickness classes (Fig. 3). Coastal areas younger than 7ka are binned into one category, the disproportionate area for this date is an edge effect.

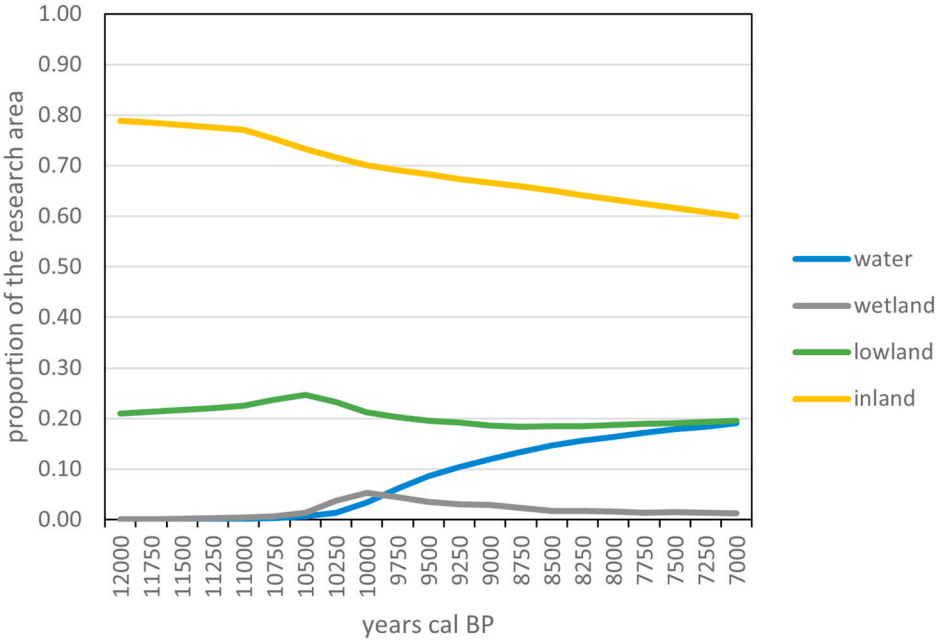

Fig. 17. Changes in proportionality of landscape zones in the eastern part of the research area over time (IM112).

number of these sites fall within the lowland landscape category. Archaeological remains from this landscape zone are expected to be slightly overrepresented around 10.5 ka, given the changing proportionality (Fig. 17), but the growth rate actually increases towards 10.25 ka. Additionally, while a good portion of coastal zones dating around 10.25 ka are theoretically accessible in the offshore (covered by 0–0.5m of Holocene sediment, Fig. 16), such sites are actually not represented in our dataset. The increased growth-rate around 10.25 ka is wholly owed to an increased number of sites and dates in onshore, higher lowland contexts (see Fig. 15). Most of these sites are not proximate to contemporaneous coastlines and were only inundated some time after 7 ka (Fig. 11), making it unlikely that there is a change in inundation-related preservation bias or accessibility at play. However, this period also sees the first appearance of Mesolithic pit hearths, which are highly visible, charcoal-rich phenomena (Niekus et al., 2022; Gehlen et al., 2020; Peeters and Niekus, 2017). Dates from pit hearths gradually become an increasing portion of the radiocarbon dataset from ca. 10.5 ka to 8.5 ka onwards (Hoebe et al., 2023a: 13). This is a real behavioural change in past human activity that could partly explain the increased growth rates at this time. Later significant deviations in regional growth rates around 9.25 ka and 7.75 ka (Fig. 14c and d) show stark differences in the eastern and western dataset. These changes do not align with significant palaeogeographic changes, and do not correlate with changes in landscape zone proportionality nor Holocene sediment cover. These may also be related to changes in past activity or differences in representativity of the radiocarbon datasets.

5.3. *Mesolithic cultural changes and inundation*

While dates-as-data results show how quantitative changes in the archaeological data correspond to the timing of inundation, this is only complementary to the identification of qualitative changes in the

archaeological record. Improving the temporal resolution and quality of inundation models as we have done in this paper contributes to a more robust framework for potential external pressures driving the timing of cultural changes during the Mesolithic than previously available (Hoebe et al., 2023a; Walker et al., 2022; Blankholm, 2020; Crombé, 2018, 2019; Street et al., 2019; Griffiths and Robinson, 2018; Waddington, 2015; Robinson et al., 2013).

The onset of the Holocene sees the rapid expansion of sites associated with the late Palaeolithic Ahrensburgian into Scandinavia (Riede, 2013). Despite this, Early Mesolithic sites in the countries surrounding the North Sea Basin continue to show similarities to the Ahrensburgian in lithic tool production (Street et al., 2019; Vermeersch, 2011; De Bie and Vermeersch, 1998). In the Early Holocene environmental context, such sites differentiate in the toolkit and projectile point types, and are commonly referred to as 'long blade' assemblage types (AT). These ATs are recognised in Britain, the Benelux and West Germany, up to ca. 10.8 ka, i.e. the end of the Preboreal (Conneller, 2021; Street et al., 2019; Cziesla, 2015; De Bie and Vermeersch, 1998). Largely contemporaneous, from the start of the Preboreal onwards, 'Star Carr' ATs are recognised in Britain (Conneller, 2021; Conneller and Overton, 2018; Reynier, 2005), and across Northwest Europe (Cziesla, 2015) and southern Scandinavia (Sørensen et al., 2018).

However, during the 11th millennium cal BP diversification in Mesolithic ATs is observed on either side of the North Sea. The onset of the Boreal at 10.8 ka, sees climatic changes and the expansion of hazel into northwest Europe. Around this time, Deepcar ATs appear in Britain (Conneller, 2021), while on the continent Neerharen ATs (Benelux, Northwest Germany) and the earliest Beuronian ATs (Southwest Germany) are recognised around this time (Crombé, 2018; Cziesla, 2015). As discussed above, the late 11th millennium cal BP sees unprecedented marine transgressions, first in the Oyster Grounds region (10.5–10ka), then in the Southern Bight (10.25 ka onward). This period sees further diversification in the Mesolithic with the first appearance of 'narrow--blade' (Waddington, 2015) and Horsham ATs in Britain (Conneller, 2021) as well as Ourlaine in Northern France and Belgium, all starting around 10.5 ka (Crombé, 2019). At 10.25 ka Verrebroek/Cinru ATs appear in Benelux, west and north Germany and Denmark (Crombé, 2019; Deeben and Niekus, 2016b). This period also marks the first appearance of the Mesolithic pit hearth phenomenon (Hoebe et al., 2023a; Niekus, 2022; Gehlen et al., 2020; Niekus, 2022, 2022; Peeters and Niekus, 2017). As discussed above, the Northwest of the research area also showed significantly higher growth rates in the radiocarbon dataset (Figs. 14 and 4.2). The onset of these widespread changes in behaviour on continental Mesolithic sites follows the abrupt cooling event known as the 10.3 ka event (Bond et al., 1997, 2001) and coincides with the highest inundation rate in our model outcome, associated with the loss of the North Frisian Peninsula (4.1). Perhaps these contemporaneous changes in material culture and behaviour mark adaptations to new conditions caused by climate change and/or sea-level rise. Sea level rise may have hampered interaction between groups on either side of inundating areas of Doggerland. Later significant growth rate differences at 9.5–9 ka and 8-7.5 ka onwards also correspond to the appearance of new ATs in continental northwest Europe. The transition to the middle Mesolithic Rhine-Meuse-Scheldt ATs and the transition to Late Mesolithic ATs respectively correspond to these phases of growth in our dataset (Crombé, 2019; Deeben and Niekus, 2016b).

6. Conclusions

The improved inundation model presented here provides valuable insights into the timing and extents of Early Holocene transgressions, which are essential to understanding related cultural changes in the Early and Middle Mesolithic. The models show the disappearance of most of Doggerland under the North Sea during the 11th and 10th millennia BP. With peaking inundation rates between 10.25 and 10 ka cal BP, and key drowning events timing >500 yr500y earlier than in previous inundation modelling. These correspond to qualitative changes in Mesolithic assemblages, as well as changes in the quantitative (radiocarbon) data.

The most significant improvement upon previous inundation models is the construction of a paleoDEM for the eastern part of the southern North Sea, which provides an approximation of the elevation at the time of inundation, excluding later Holocene sediment and erosion overprints present in bathymetric models. Sea level surfaces (SLS) based on Britain-optimised and South Scandinavia-optimised GIA (Shennan et al., 2018; Vink et al., 2007) provided continuous values of relative sea level across the Early Holocene, allowing for simple raster calculation based inundation model output. Corrections to the DEM for tectonic background subsidence and pre-inundation peat growth further improved the inundation model. The effect of the different model components on inundation model output was compared, in terms of the timing, area and extent of inundations in Doggerland, showing how particular inundation model choices lead to comparatively earlier or later inundation. Besides the expansion of paleoDEM datasets to also include the west of the study region, future improvements in inundation modelling could include more sophisticated spatially variable sedimentation and erosion rasters (e.g. for the tidal systems in the Outer Silver Pit, for Early Holocene beaches against Dogger Island) and explicit and tidal amplitude rasters per timestep (e.g. before and after marine connections established), especially for estuarine environments. Additionally, more sophisticated modelling of sea-level-rise-driven groundwater-level-rise would significantly improve insight into paludification and extent of back-barrier wetland formation. While higher spatial (1 × 1 km) and temporal resolution (centennial, decadal) output are feasible, this would result in an imprudent level of illusory accuracy given the current uncertainty margins in the input data and corrections.

Key periods and regions of significant growth could be identified in the archaeological radiocarbon dataset that correspond to phases of high inundation rate in our inundation model. However, the role of taphonomy (loss, mixing) and accessibility in shaping the quantitative spatiotemporal patterns of archaeological (radiocarbon) data is very important. Especially in regions with complex histories of sedimentation and erosion as a result of inundation, insight into landscape taphonomy is essential. By constructing case-study-specific taphonomic corrections large scale spatiotemporal patterns of past human behaviour can potentially be disentangled from the patterns of research, preservation and accessibility bias. We argue that inundation models can contribute to such corrections for the Early Holocene Northwest Europe by providing information on the distribution and thickness of post-transgression sediments both on and offshore, as well as the positioning of coastlines and the relative proportion of past landscape zones.

Data availability

Data, R and python scripts are available in the electronic supplements to this paper and on the first author's github (https://github.com/pirhoebe/InundationDoggerlandHunterGatherers).

Funding

This study is part of the first author's PhD research, financed by the University of Groningen.

CRediT authorship contribution statement

P.W. Hoebe: Conceptualization, Data curation, Formal analysis, Investigation, Methodology, Resources, Software, Visualization, Writing – original draft, Writing – review & editing. **K.M. Cohen:** Conceptualization, Data curation, Methodology, Resources, Validation, Writing – review & editing. **F.S. Busschers:** Conceptualization, Methodology, Resources, Software, Writing – original draft. **S. van Heteren:** Conceptualization, Resources, Writing – review & editing. **J.H.M.**

Peeters: Conceptualization, Supervision, Validation, Writing – review & editing.

Declaration of competing interest

The authors declare that they have no known competing financial interests or personal relationships that could have appeared to influence the work reported in this paper.

Acknowledgements

We would like to express our gratitude to the following people. Marc Hijma and Kim de Wit for correspondence and helpful discussion concerning sea level indication points and SLS construction. Vince Gaffney, Simon Fitch, Phil Murgatroyd for their correspondence about English seafloor data. Jasper Verhaegen (DO Vlaanderen) and Maikel De Clerq for their correspondence about paleoDEM construction for Belgium and for supplying data. Stijn Arnoldussen for the helpful discussions and supervision. The suggestions made by three anonymous reviewers helped improve the text.

Appendix A. Supplementary data

Supplementary data to this article can be found online at https://doi.org/10.1016/j.quaint.2024.05.006.

References

Abegunrin, A., Hepp, D.A., Gugliotta, M., Mörz, T., 2023. The submerged palaeo-Ems river in the Quaternary stratigraphic context of the German North Sea. Holocene 33, 1504–1516.
Amkreutz, L., Verpoorte, A., Waters-Rist, A., Niekus, M., Van Heekeren, V., Van Der Merwe, A., Van Der Plicht, H., Glimmerveen, J., Stapert, D., Johansen, L., 2018. What lies beneath . . . Late Glacial human occupation of the submerged North Sea landscape. Antiquity 92, 22–37.
Arfai, J., Franke, D., Lutz, R., Reinhardt, L., Kley, J., Gaedicke, C., 2018. Rapid Quaternary subsidence in the northwestern German North Sea. Sci. Rep. 8, 11524.
Attenbrow, V., Hiscock, P., 2015. Dates and demography: are radiometric dates a robust proxy for long-term prehistoric demographic change? Archaeol. Ocean. 50, 30–36.
Bailey, G., Galanidou, N., Peeters, H., Jöns, H., Mennenga, M., 2020a. The archaeology of Europe's drowned landscapes: introduction and overview. Coastal Research Library 35, 1–23.
Bailey, G., Hardy, K., 2021. Coastal prehistory and submerged landscapes: Molluscan resources, shell-middens and underwater investigations. Quat. Int. 584, 1–8.
Bailey, G., Momber, G., Bell, M., Tizzard, L., Hardy, K., Bicket, A., Tidbury, L., Benjamin, J., Hale, A., 2020b. Great Britain: the Intertidal and Underwater Archaeology of Britain's Submerged Landscapes. Coast. Res. Library 35, 1–23.
Ballin, T.B., 2018. Reindeer Hunters at Howburn Farm, South Lanarkshire: a Late Hamburgian Settlement in Southern Scotland - its Lithic Artefacts and Natural Environment. Archaeopress Publishing, Oxford.
Becerra-Valdivia, L., Leal-Cervantes, R., Wood, R., Higham, T., 2020. Challenges in sample processing within radiocarbon dating and their impact in 14C-dates-as-data studies. J. Archaeol. Sci. 113, 105043.
Behre, K., 2007. A new Holocene sea-level curve for the southern North Sea. Boreas 36, 82–102.
Benjamini, Y., Hochberg, Y., 1995. Controlling the false discovery rate: a practical and Powerful approach to multiple testing. J. R. Statist. Soc. B 57 (1), 289–300.
Bird, D., Miranda, L., Vander Linden, M., Robinson, E., Bocinsky, R.K., Nicholson, C., Capriles, J.M., Finley, J.B., Gayo, E.M., Gil, A., d'Alpoim Guedes, J., Hoggarth, J.A., Kay, A., Loftus, E., Lombardo, U., Mackie, M., Palmisano, A., Solheim, S., Kelly, R.L., Freeman, J., 2022. p3k14c, a synthetic global database of archaeological radiocarbon dates. Sci. Data 9, 27.
Blankholm, H.P., 2020. In the wake of the wake. An investigation of the impact of the Storegga tsunami on the human settlement of inner Varangerfjord, northern Norway. Quat. Int. 549, 65–73.
Bluhm, L.E., Surovell, T.A., 2019. Validation of a global model of taphonomic bias using geologic radiocarbon ages. Quat. res. 91, 325–328.
Bond, G., Kromer, B., Beer, J., Muscheler, R., Evans, M.N., Showers, W., Hoffmann, S., Lotti-Bond, R., Hajdas, I., Bonani, G., 2001. Persistent solar influence on North Atlantic climate during the Holocene. Science 294, 2130–2136.
Bond, G., Showers, W., Cheseby, M., Lotti, R., Almasi, P., Priore, P., Cullen, H., Hajdas, I., Bonani, G., Bond, G., Showers, W., Cheseby, M., Lotti, R., Almasi, P., Priore, P., Cullen, H., Hajdas, I., Bonani, G., 1997. A Pervasive millennial-scale Cycle in North Atlantic Holocene and glacial climates. Science 278, 1257–1266.
Bradley, S.L., 2011. Using Sea-Level and Land Motion Data to Develop an Improved Glacial Isostatic Adjustment Model for the British Isles. Available at: Durham E-Theses Online:. Durham University http://etheses.dur.ac.uk/600/.
Bradley, S.L., Milne, G.A., Shennan, I., Edwards, R., 2011. An improved glacial isostatic adjustment model for the British Isles. J. Quaternary Sci. 26, 541–552.
Briggs, K., Thomson, K., Gaffney, V., 2007. A geomorphological investigation of submerged depositional features within the outer Silver pit, Southern North sea (chapter 5). In: Thomson, V. Gaffney K., Fitch, S. (Eds.), Mapping Doggerland: the Mesolithic Landscapes of the Southern North Sea. Archaeopress Publishing, Oxford.
Bronk Ramsey, C., 2017. Methods for summarizing radiocarbon datasets. Radiocarbon 59, 1809–1833.
Brooks, A.J., Bradley, S.L., Edwards, R.J., Goodwyn, N., 2011. The palaeogeography of Northwest Europe during the last 20,000 years. J. Maps 7, 573–587.
Brown, W.A., 2017. The past and future of growth rate estimation in demographic temporal frequency analysis: Biodemographic interpretability and the ascendance of dynamic growth models. J. Archaeol. Sci. 80, 96–108.
Bungenstock, F., Freund, H., Bartholomä, A., 2022. Holocene relative sea-level data for the East Frisian barrier coast, NW Germany, southern North Sea – CORRIGENDUM. Neth. J. Geosci. 101, e2.
Busschers, F.S., Kasse, C., Van Balen, R.T., Vandenberghe, J., Cohen, K.M., Weerts, H.J. T., Wallinga, J., Johns, C., Cleveringa, P., Bunnik, F.P.M., 2007. Late Pleistocene evolution of the Rhine-Meuse system in the southern North Sea basin: imprints of climate change, sea-level oscillation and glacio-isostacy. Quat. Sci. Rev. 26, 3216–3248.
Carleton, W.C., Groucutt, H.S., 2021. Sum things are not what they seem: problems with point-wise interpretations and quantitative analyses of proxies based on aggregated radiocarbon dates. Holocene 31, 630–643.
Carlson, A.E., Clark, P.U., 2012. Ice sheet sources of sea level rise and freshwater discharge during the last deglaciation. Rev. Geophys. 50, 2011RG000371.
Cartelle, V., Barlow, N.L.M., Hodgson, D.M., Busschers, F.S., Cohen, K.M., Meijninger, B. M.L., Van Kesteren, W.P., 2021. Sedimentary architecture and landforms of the late Saalian (MIS 6) ice sheet margin offshore of The Netherlands. Earth Surf. Dynam 9, 1399–1421.
Clark, C.D., Ely, J.C., Hindmarsh, R.C.A., Bradley, S., Ignéczi, A., Fabel, D., Ó Cofaigh, C., Chiverrell, R.C., Scourse, J., Benetti, S., Bradwell, T., Evans, D.J.A., Roberts, D.H., Burke, M., Callard, S.L., Medialdea, A., Saher, M., Small, D., Smedley, R.K., Gasson, E., Gregoire, L., Gandy, N., Hughes, A.L.C., Ballantyne, C., Bateman, M.D., Bigg, G.R., Doole, J., Dove, D., Duller, G.A.T., Jenkins, G.T.H., Livingstone, S.L., McCarron, S., Moreton, S., Pollard, D., Praeg, D., Sejrup, H.P., Van Landeghem, K.J. J., Wilson, P., 2022. Growth and retreat of the last British–Irish Ice Sheet, 31 000 to 15 000 years ago: the BRITICE-CHRONO reconstruction. Boreas 51, 1–60.
Cohen, K.M., 2005. 3D Geostatistical interpolation and geological interpretation of paleo-groundwater rise in the Holocene coastal prism in The Netherlands. In: Giosan, L., Bhattacharya, J.P. (Eds.), River Deltas–Concepts, Models, and Examples.
Cohen, K.M., Cartelle, V., Barnett, R., Busschers, F.S., Barlow, N.L.M., 2022. Last interglacial sea-level data points from Northwest Europe. Earth Syst. Sci. Data 14, 2895–2937.
Cohen, K.M., Gibbard, P.L., 2019. Global chronostratigraphical correlation table for the last 2.7 million years, version 2019 QI-500. Quat. Int. 500, 20–31.
Cohen, K.M., Gibbard, P.L., Weerts, H.J.T., 2014. North Sea palaeogeographical reconstructions for the last 1 Ma. Neth. J. Geosci. 93, 7–29.
Cohen, K.M., MacDonald, K., Joordens, J.C.A., Roebroeks, W., Gibbard, P.L., 2012. The earliest occupation of north-west Europe: a coastal perspective. Quat. Int. 271, 70–83.
Cohen, K.M., Westley, K., Erkens, G., P, H.M., Weerts, H.J., 2017. The North sea. Submerged Landscapes of the European Continental Shelf: Quaternary Paleoenvironments, pp. 1–533.
Coles, B.J., 1998. Doggerland: a speculative survey. Proc. Prehist. Soc. 64, 45–81.
Conneller, C., 2021. The Mesolithic in Britain: Landscape and Society in Times of Change, first ed. Routledge, London.
Conneller, C., Overton, N.J., 2018. The British mesolithic context. In: Conneller, N. Milner C., Taylor, B. (Eds.), Star Carr: A Persistent Place in a Changing World, vol. 1. White Rose University Press, pp. 275–303.
Contreras, D.A., Codding, B.F., 2023. Landscape taphonomy predictably complicates demographic reconstruction. J. Archaeol. Method Theor. 1–17. https://doi.org/10.1007/s10816-023-09634-5.
Contreras, D.A., Meadows, J., 2014. Summed radiocarbon calibrations as a population proxy: a critical evaluation using a realistic simulation approach. J. Archaeol. Sci. 52, 591–608.
Cotterill, C.J., Phillips, E., James, L., Forsberg, C.F., Tjelta, T.I., Carter, G., Dove, D., 2017. The evolution of the Dogger Bank, North Sea: a complex history of terrestrial, glacial and marine environmental change. Quat. Sci. Rev. 171, 136–153.
Crema, E.R., 2022. Statistical inference of prehistoric demography from frequency distributions of radiocarbon dates: a review and a guide for the perplexed. J. Archaeol. Method Theor 29, 1387–1418.
Crema, E.R., Bevan, A., 2021. Inference from large sets of radiocarbon dates: software and methods. Radiocarbon 63, 23–39.
Crema, E.R., Bevan, A., Shennan, S., 2017. Spatio-temporal approaches to archaeological radiocarbon dates. J. Archaeol. Sci. 87, 1–9.
Crombé, P., 2018. Abrupt cooling events during the Early Holocene and their potential impact on the environment and human behaviour along the southern North Sea basin (NW Europe). J. Quat. Sci. 33, 353–367.
Crombé, P., 2019. Mesolithic projectile variability along the southern North Sea basin (NW Europe): hunter-gatherer responses to repeated climate change at the beginning of the Holocene. PLoS One 14, e0219094.
Crombé, P., Robinson, E., 2017. Human resilience to Lateglacial climate and environmental change in the Scheldt basin (NW Belgium). Quat. Int. 428, 50–63.
Cziesla, E., 2015. Grenzen im Wald - Stabilität und Kontinuität während des Mesolithikums in der Mitte Europas. Verlag Marie Leidorf GmbH, Rahden Westfalen.

De Bie, M., Vermeersch, P.M., 1998. Pleistocene - Holocene transition in Benelux. Quat. Int. 49–50, 29–43.
De Clercq, M., 2018. Drowned landscapes of the Belgian continental shelf. Implications for Northwest European Landscape Evolution and Preservation Potential for Submerged Heritage. Ghent University.
De Clercq, M., Chademenos, V., Van Lancker, V., Missiaen, T., 2016. A high-resolution DEM for the top-palaeogene surface of the Belgian continental shelf. J. Maps 12, 1047–1054.
De Haas, H., Van Weering, T.C.E., 1997. Recent sediment accumulation, organic carbon burial and transport in the northeastern North Sea. Mar. Geol. 136, 173–187.
Deeben, J., Niekus, M., 2016a. De federmesser-traditie. In: Amkreutz, L.W.S.W., Brounen, F., Deeben, J., Machiels, R., Smit, M.-F. van Oorsouw B., Altena, E. (Eds.), *Vuursteen verzameld: Over het zoeken en onderzoeken van steentijdvondsten en -vindplaatsen*, Rijksdienst voor het Cultureel Erfgoed, Amersfoort.
Deeben, J., Niekus, M., 2016b. Mesolithicum. In: Amkreutz, L.W.S.W., Brounen, F., Deeben, J., Machiels, R., Smit, M.-F. van Oorsouw B., Altena, E. (Eds.), *Vuursteen verzameld: Over het zoeken en onderzoeken van steentijdvondsten en -vindplaatsen*, Rijksdienst voor het Cultureel Erfgoed, Amersfoort.
Eisma, D., Mook, W.G., Laban, C., 1981. An early Holocene tidal flat in the southern Bight. In: Nio, S.-D., Shüttenhelm, R.T.E., Van Weering, Tj C.E. (Eds.), Holocene Marine Sedimentation in the North Sea Basin. Wiley, pp. 229–237.
Emery, A.R., Hodgson, D.M., Barlow, N.L.M., Carrivick, J.L., Cotterill, C.J., Mellett, C.L., Booth, A.D., 2019. Topographic and hydrodynamic controls on barrier retreat and preservation: an example from Dogger Bank, North Sea. Mar. Geol. 416, 105981.
Fairbanks, R.G., 1989. A 17,000-year glacio-eustatic sea level record: influence of glacial melting rates on the Younger Dryas event and deep-ocean circulation. Nature 342, 637–642.
Fitch, S., Gaffney, V., Harding, R., Walker, J., Bates, R., Bates, M., Fraser, A., 2022. A description of palaeolandscape features in the southern North Sea (chapter 3). In: Gaffney, V., Fitch, S. (Eds.), Europe's Lost Frontiers. Context And Methodology, Archaeopress Publishing, Oxford.
Fitch, S., Gaffney, V., Thomson, K., 2007. In: Sight of Doggerland: from Speculative Survey to Landscape Exploration. IA.
Fitch, S., Thomson, K., Gaffney, V., 2005. Late Pleistocene and Holocene depositional systems and the palaeogeography of the Dogger Bank, North Sea. Quat. res. 64, 185–196.
Gaffney, V., Fitch, S., Bates, M., Ware, R.L., Kinnaird, T., Gearey, B., Hill, T., Telford, R., Batt, C., Stern, B., Whittaker, J., Davies, S., Sharada, M.B., Everett, R., Cribdon, R., Kistler, L., Harris, S., Kearney, K., Walker, J., Muru, M., Hamilton, D., Law, M., Finlay, A., Bates, R., Allaby, R.G., 2020. Multi-proxy characterisation of the Storegga tsunami and its impact on the early Holocene landscapes of the Southern North sea. Geosciences 10, 1–19.
Gaffney, V.G., Fitch, S. (Eds.), 2022. Europe's Lost Frontiers: Context And Methodology. Archaeopress Publishing, Oxford.
Gaffney, V., Thomson, K., Fitch, S. (Eds.), 2007. Mapping Doggerland: the Mesolithic Landscapes of the Southern North Sea. Archaeopress Publishing, Oxford.
Gehlen, B., Eckmeier, E., Gerken, K., Werner, S., Zander, A., 2020. Mesolithic pits in Germany - a first compilation. In: Gehlen, A. Zander B., Gramsch, B. (Eds.), *From the Early Preboreal to the Subboreal Period – Current Mesolithic Research in Europe: Studies in Honour of Bernhard Gramsch = Vom Frühen Präboreal Bis Zum Subboreal – Aktuelle Forschungen Zum Mesolithikum in Europa: Studien Zu Ehren von Bernhard Gramsch*, Welt und Erde Verlag. Kerpen-Loogh.
Griffiths, S., Robinson, E., 2018. The 8.2 ka BP Holocene climate change event and human population resilience in northwest Atlantic Europe. Quat. Int. 465, 251–257.
Gupta, S., Collier, J.S., Garcia-Moreno, D., Oggioni, F., Trentesaux, A., Vanneste, K., De Batist, M., Camelbeeck, T., Potter, G., Van Vliet-Lanoë, B., Arthur, J.C.R., 2017. Two-stage opening of the Dover Strait and the origin of island Britain. Nat. Commun. 8, 15101.
Gupta, S., Collier, J.S., Palmer-Felgate, A., Potter, G., 2007. Catastrophic flooding origin of shelf valley systems in the English Channel. Nature 448, 342–345.
Gyllencreutz, R., 2005. Late Glacial and Holocene paleoceanography in the Skagerrak from high-resolution grain size records. Palaeogeogr. Palaeoclimatol. Palaeoecol. 222, 344–369.
Heaton, T.J., 2022. Non-parametric calibration of multiple related radiocarbon determinations and their calendar age summarisation. J. Roy. Stat. Soc. C Appl. Stat. 71, 1918–1956.
Hijma, M.P., Cohen, K.M., 2010. Timing and magnitude of the sea-level jump preluding the 8200 yr event. Geology 38, 275–278.
Hijma, M.P., Cohen, K.M., 2011. Holocene transgression of the Rhine river mouth area, The Netherlands/Southern North Sea: palaeogeography and sequence stratigraphy: Holocene transgression of the Rhine river mouth area, The Netherlands/Southern North Sea. Sedimentology 58, 1453–1485.
Hijma, M.P., Cohen, K.M., 2019. Holocene sea-level database for the Rhine-Meuse Delta, The Netherlands: implications for the pre-8.2 ka sea-level jump. Quat. Sci. Rev. 214, 68–86.
Hijma, M.P., Cohen, K.M., Roebroeks, W., Westerhoff, W.E., Busschers, F.S., 2012. Pleistocene Rhine-Thames landscapes: geological background for hominin occupation of the southern North Sea region. J. Quaternary Sci. 27, 17–39.
Hoebe, P.W., Peeters, J.H.M., Arnoldussen, S., 2023a. Parsing prehistoric patterns: prospects and limitations of a big radiocarbon dataset for understanding the impact of climate on Late Palaeolithic and Mesolithic populations in northwest Europe (16–7.5 ka cal BP). J. Archaeol. Sci.: Reports 49, 103944.
Hoebe, P.W., Peeters, J.H.M., Arnolddusen, S., 2023b. Reply to Vermeersch's comment on Hoebe *et al.* 2023. Parsing prehistoric patterns. J. Archaeol. Sci.: Reports 52, 104229.
Jelgersma, S., 1961. Holocene sea level changes in the Netherlands. Dissertation Leiden University.
Jelgersma, S., 1982. Sea-Level changes in the North Sea basin. In: Schüttenhelm, O.E., Wiggers, A.E. (Eds.), The Quaternary History of the North Sea. Acta Universitatis Upsaliensis Symposia Universitatis Upsaliensis Annum Quingentesimum Celebrantis, pp. 233–248.
Jöns, H., Lüth, F., Mahlstedt, S., Goldhammer, J., Hartz, S., Kühn, H.J., 2020. Germany: submerged sites in the south-western baltic sea and the wadden sea. Coastal Research Library 35, 95–123.
Kibblewhite, M., Tóth, G., Hermann, T., 2015. Predicting the preservation of cultural artefacts and buried materials in soil. Sci. Total Environ. 529, 249–263.
Kooi, H., Johnston, P., Lambeck, K., Smither, C., Molendijk, Ronald, 1998. Geological causes of recent (~100 yr) vertical land movement in The Netherlands. Tectonophysics 299, 297–316.
Koster, K., Stafleu, J., Cohen, K.M., 2017. Generic 3D interpolation of Holocene base-level rise and provision of accommodation space, developed for The Netherlands coastal plain and infilled palaeovalleys. Basin Res. 29, 775–797.
Kuchar, J., Milne, G., Hubbard, A., Patton, H., Bradley, S., Shennan, I., Edwards, R., 2012. Evaluation of a numerical model of the British–Irish ice sheet using relative sea-level data: implications for the interpretation of trimline observations. J Quaternary Science 27, 597–605.
Laban, C., Cameron, T.D.J., Schüttenhelm, R.T.E., 1984. Geologie van het kwartair in de zuidelijke bocht van de Noordzee. Mededelingen van de Werkgroepvoor Tertiaire en Kwartaire Geologie 21, 139–154.
Lambeck, K., 1993. Glacial rebound of the British Isles-I. Preliminary model results. Geophys. J. Int. 115, 941–959.
Lambeck, K., 1995. Late devensian and Holocene shorelines of the British isles and north Sea from models of glacio-hydro-isostatic rebound. J. Geol. Soc. 152, 437–448.
Lambeck, K., Rouby, H., Purcell, A., Sun, Y., Sambridge, M., 2014. Sea level and global ice volumes from the last glacial maximum to the Holocene. Proc. Natl. Acad. Sci. U. S.A. 111, 15296–15303.
Lambeck, K., Smither, C., Johnston, P., 1998. Sea-level change, glacial rebound and mantle viscosity fornorthern Europe. Geophys. J. Int. 134, 102–144.
Larcombe, P., Ward, I.A.K., 2018. Comment on Williams et al., 2018, Sea-level change and demography during the last glacial termination and early Holocene across the Australian continent. Quat. Sci. Rev. 201, 501–504.
Lawrence, D., Palmisano, A., de Gruchy, M.W., 2021. Collapse and continuity: a multi-proxy reconstruction of settlement organization and population trajectories in the Northern Fertile Crescent during the 4.2kya Rapid Climate Change event. PLoS One 16, 1–20.
Lehmkuhl, F., Nett, J.J., Pötter, S., Schulte, P., Sprafke, T., Jary, Z., Antoine, P., Wacha, L., Wolf, D., Zerboni, A., Hošek, J., Marković, S.B., Obreht, I., Sümegi, P., Veres, D., Zeeden, C., Boemke, B., Schaubert, V., Viehweger, J., Hambach, U., 2021. Loess landscapes of Europe – mapping, geomorphology, and zonal differentiation. Earth Sci. Rev. 215, 103496.
Lisiecki, L.E., Raymo, M.E., 2005. A Pliocene-Pleistocene stack of 57 globally distributed benthic δ^{18}O records. Paleoceanography 20, 2004PA001071.
Louwe Kooijmans, L.P., 1971. Mesolithic Bone and Antler Implements from the North Sea and from the Netherlands. Berichten Rijksdienst Voor Het Oudheidkundig Bodemonderzoek, pp. 27–73.
Maier, A., 2015. The Central European Magdalenian: Regional Diversity and Internal Variability. Springer Netherlands, Dordrecht.
Massey, A.C., Gehrels, W.R., Charman, D.J., Milne, G.A., Peltier, W.R., Lambeck, K., Selby, K.A., 2008. Relative sea-level change and postglacial isostatic adjustment along the coast of south Devon, United Kingdom. J Quaternary Science 23, 415–433.
Meijles, E.W., Kiden, P., Streurman, H.J., van der Plicht, J., Vos, P.C., Gehrels, W.R., Kopp, R.E., 2018. Holocene relative mean sea-level changes in the Wadden Sea area, northern Netherlands. J. Quat. Sci. 33, 905–923.
Milner, N., Craig, O.E., Bailey, G.N. (Eds.), 2007. Shell Middens in Atlantic Europe. Oxbow Books.
Mithen, S., Wicks, K., 2021. Population level models for testing hunter-gatherer resilience and settlement response to the combined impact of abrupt climatic events and sea level change: a case study from the Holocene of northern Britain. Quat. Sci. Rev. 265, 107027.
Momber, G., Rich, S., 2015. Postglacial human dispersal across the North-West European landscape. Zeitschrift für maritime und limnische Archäologie und Kulturgeschichte 15 (1), 4–14.
Niekus, M.J.L.Th., 2022. Marking mesolithic mobility: the curious case of pit hearth clusters in the low countries (chapter 7). In: Sobkowiak-Tabaka, I., Diachenko, A., Wiśniewski, A. (Eds.), Quantifying Stone Age Mobility: Scales and Parameters. Springer International Publishing, Cham, pp. 153–191.
Nyland, A.J., Walker, J., Warren, G., 2021. Evidence of the Storegga tsunami 8200 BP? An archaeological review of impact after a large-scale marine event in mesolithic northern Europe. Front. Earth Sci. 9, 1–15.
Özmaral, A., Abegunrin, A., Keil, H., Hepp, D.A., Schwenk, T., Lantzsch, H., Mörz, T., Spiess, V., 2022. The Elbe palaeovalley: evolution from an ice-marginal valley to a sedimentary trap (SE North Sea). Quat. Sci. Rev. 282, 107453.
Palmisano, A., Lawrence, D., de Gruchy, M.W., Bevan, A., Shennan, S., 2021. Holocene regional population dynamics and climatic trends in the Near East: a first comparison using archaeo-demographic proxies. Quat. Sci. Rev. 252, 106739.
Peeters, H., Amkreutz, L., 2020. The Netherlands: probing into the submerged prehistoric archaeology, landscapes and palaeontology of the Dutch continental shelf. Coastal Research Library 35, 157–174.
North sea prehistoric research and management framework (NSPRMF) 2009. In: Peeters, H., Murphy, P., Flemming, N. (Eds.), 2009. Rijksdienst Voor Het Cultureel Erfgoed English Heritage, Amersfoort.

Peeters, H., Niekus, M.J.L.Th., 2017. Mesolithic pit hearths in the northern Netherlands - function, time-depth and behavioural context. Acres de la Séances de la Société Préhistorique Française 12, 111–132.
Peeters, H., Sturt, F., Westley, K., 2020. The atlantic margin and the North sea: introduction. Coastal Research Library 35, 143–155.
Peeters, J.H.M., Amkreutz, L.W.S.W., Cohen, K.M., Hijma, M.P., 2019. North Sea Prehistory Research and Management Framework (NSPRMF) 2019. NAR063. Cultural Heritage Agency, Amersfoort.
Peeters, J.H.M., Momber, G., 2014. The southern North Sea and the human occupation of Northwest Europe after the last glacial maximum. Neth. J. Geosci. 93, 55–70.
Peltier, W.R., 2002. On eustatic sea level history: last Glacial Maximum to Holocene. Quat. Sci. Rev. 21, 377–396.
Perreault, C., 2019. The Quality of the Archaeological Record. University of Chicago Press.
Pettitt, P., White, M., 2012. The British Palaeolithic. Routledge, London.
Phillips, E., Cotterill, C., Johnson, K., Crombie, K., James, L., Carr, S., Ruiter, A., 2018. Large-scale glacitectonic deformation in response to active ice sheet retreat across Dogger Bank (southern central North Sea) during the Last Glacial Maximum. Quat. Sci. Rev. 179, 24–47.
Pierik, H.J., Moree, J.I.M., Van Der Werf, K.M., Roelofs, L., Albernaz, M.B., Wilbers, A., Van Der Valk, B., Van Dinter, M., Hoek, W.Z., De Haas, T., Kleinhans, M.G., 2023. Vegetation and peat accumulation steer Holocene tidal–fluvial basin filling and overbank sedimentation along the Old Rhine River, The Netherlands. Sedimentology 70, 179–213.
Pieters, M., Missiaen, T., De Clercq, M., Demerre, I., Van Haelst, S., 2020. Belgium: prehistoric and protohistoric archaeology in the intertidal and subtidal zones of the North Sea. Coastal Research Library 35, 175–187.
Posth, C., Yu, H., Ghalichi, A., Rougier, H., Crevecoeur, I., Huang, Y., Ringbauer, H., Rohrlach, A.B., Nägele, K., Villalba-Mouco, V., Radzeviciute, R., Ferraz, T., Stoessel, A., Tukhbatova, R., Drucker, D.G., Lari, M., Modi, A., Vai, S., Saupe, T., Scheib, C.L., Catalano, G., Pagani, L., Talamo, S., Fewlass, H., Klaric, L., Morala, A., Rué, M., Madelaine, S., Crépin, L., Caverne, J.-B., Bocaege, E., Ricci, S., Boschin, F., Bayle, P., Maureille, B., Le Brun-Ricalens, F., Bordes, J.-G., Oxilia, G., Bortolini, E., Bignon-Lau, O., Debout, G., Orliac, M., Zazzo, A., Sparacello, V., Starnini, E., Sineo, L., Van Der Plicht, J., Pecqueur, L., Merceron, G., Garcia, G., Leuvrey, J.-M., Garcia, C.B., Gómez-Olivencia, A., Połtowicz-Bobak, M., Bobak, D., Le Luyer, M., Storm, P., Hoffmann, C., Kabaciński, J., Filimonova, T., Shnaider, S., Berezina, N., González-Rabanal, B., González Morales, M.R., Marín-Arroyo, A.B., López, B., Alonso-Llamazares, C., Ronchitelli, A., Polet, C., Jadin, I., Cauwe, N., Soler, J., Coromina, N., Rufí, I., Cottiaux, R., Clark, G., Straus, L.G., Julien, M.-A., Renhart, S., Talaa, D., Benazzi, S., Romandini, M., Amkreutz, L., Bocherens, H., Wißing, C., Villotte, S., De Pablo, J.F.-L., Gómez-Puche, M., Esquembre-Bebia, M.A., Bodu, P., Smits, L., Souffi, B., Jankauskas, R., Kozakaitė, J., Cupillard, C., Benthien, H., Wehrberger, K., Schmitz, R.W., Feine, S.C., Schüler, T., Thevenet, C., Grigorescu, D., Lüth, F., Kotula, A., Piezonka, H., Schopper, F., Svoboda, J., Sázelová, S., Chizhevsky, A., Khokhlov, A., Conard, N.J., Valentin, F., Harvati, K., Semal, P., Jungklaus, B., Suvorov, A., Schulting, R., Moiseyev, V., Mannermaa, K., Buzhilova, A., Terberger, T., Caramelli, D., Altena, E., Haak, W., Krause, J., 2023. Palaeogenomics of upper palaeolithic to neolithic European hunter-gatherers. Nature 615, 117–126.
Price, M.H., Capriles, J.M., Hoggarth, J.A., Bocinsky, R.K., Ebert, C.E., Jones, J.H., 2021. End-to-end Bayesian analysis for summarizing sets of radiocarbon dates. J. Archaeol. Sci. 135, 105473.
Reimer, P.J., Austin, W.E.N., Bard, E., Bayliss, A., Blackwell, P.G., Bronk Ramsey, C., Butzin, M., Cheng, H., Edwards, R.L., Friedrich, M., Grootes, P.M., Guilderson, T.P., Hajdas, I., Heaton, T.J., Hogg, A.G., Hughen, K.A., Kromer, B., Manning, S.W., Muscheler, R., Palmer, J.G., Pearson, C., Van Der Plicht, J., Reimer, R.W., Richards, D.A., Scott, E.M., Southon, J.R., Turney, C.S.M., Wacker, L., Adolphi, F., Büntgen, U., Capano, M., Fahrni, S.M., Fogtmann-Schulz, A., Friedrich, R., Köhler, P., Kudsk, S., Miyake, F., Olsen, J., Reinig, F., Sakamoto, M., Sookdeo, A., Talamo, S., 2020. The IntCal20 northern hemisphere radiocarbon age calibration curve (0-55 cal kBP). Radiocarbon 62, 725–757.
Reynier, M.J., 2005. Early Mesolithic Britain: Origins, Development and Directions. British Archaeological Reports. British Series, p. 393.
Riede, F., 2013. The resettlement of Northern Europe (Chapter 25). In: Jordan, V., Cummings, P., Zvelebil, M. (Eds.), The Oxford Handbook of the Archaeology and Anthropology of Hunter-Gatherers. Oxford University Press, pp. 556–581.
Robinson, E., Van Strydonck, M., Gelorini, V., Crombé, P., 2013. Radiocarbon chronology and the correlation of hunter–gatherer sociocultural change with abrupt palaeoclimate change: the Middle Mesolithic in the Rhine–Meuse–Scheldt area of northwest Europe. J. Archaeol. Sci. 40, 755–763.
Rohling, E.J., Grant, K., Bolshaw, M., Roberts, A.P., Siddall, M., Hemleben, Ch, Kucera, M., 2009. Antarctic temperature and global sea level closely coupled over the past five glacial cycles. Nature Geosci 2, 500–504.
Schaetzl, R.J., Bettis, E.A., Crouvi, O., Fitzsimmons, K.E., Grimley, D.A., Hambach, U., Lehmkuhl, F., Marković, S.B., Mason, J.A., Owczarek, P., Roberts, H.M., Rousseau, D.-D., Stevens, T., Vandenberghe, J., Zárate, M., Veres, D., Yang, S., Zech, M., Conroy, J.L., Dave, A.K., Faust, D., Hao, Q., Obreht, I., Prud'homme, C., Smalley, I., Tripaldi, A., Zeeden, C., Zech, R., 2018. Approaches and challenges to the study of loess—introduction to the LoessFest special issue. Quat. res. 89, 563–618.
Shennan, I., 2018. Sea level studies - overview. Reference Module. Earth Systems and Environmental Sciences. Elsevier. https://doi.org/10.1016/B978-0-12-409548-9.11063-2.
Shennan, I., Bradley, S.L., Edwards, R., 2018. Relative sea-Level changes and crustal movements in Britain and Ireland since the last glacial maximum. Quat. Sci. Rev. 188, 143–159.
Shennan, I., Lambeck, K., Horton, B., Innes, J., Lloyd, J., McArthur, J., Rutherford, M., 2000. Holocene Isostasy and Relative Sea-Level Changes on the East Coast of England. SP 166, pp. 275–298.
Shennan, S., Downey, S.S., Timpson, A., Edinborough, K., Colledge, S., Kerig, T., Manning, K., Thomas, M.G., 2013. Regional population collapse followed initial agriculture booms in mid-Holocene Europe. Nat. Commun. 4, 31–34.
Smith, D.E., Shi, S., Cullingford, R.A., Dawson, A.G., Dawson, S., Firth, C.R., Foster, I.D. L., Fretwell, P.T., Haggart, B.A., Holloway, L.K., Long, D., 2004. The Holocene Storegga slide tsunami in the United Kingdom. Quat. Sci. Rev. 23–24, 2291–2321.
Sørensen, M., Lübke, H., Groß, D., 2018. The early mesolithic in southern Scandinavia and northern Germany. In: Conneller, N. Milner C., Taylor, B. (Eds.), Star Carr Volume I. White Rose University Press, pp. 305–329.
Steffen, H., Kaufmann, G., 2005. Glacial isostatic adjustment of Scandinavia and northwestern Europe and the radial viscosity structure of the Earth's mantle. Geophys. J. Int. 163, 801–812.
Steffen, H., Kaufmann, G., Wu, P., 2006. Three-dimensional finite-element modeling of the glacial isostatic adjustment in Fennoscandia. Earth Planet Sci. Lett. 250, 358–375.
Steffen, H., Wu, P., 2011. Glacial isostatic adjustment in Fennoscandia—a review of data and modeling. J. Geodyn. 52, 169–204.
Street, M., Baales, M., Cziesla, E., Heinen, M., Terberger, T., 2002. Final paleolithic and mesolithic research in reunified Germany. J. World PreHistory 14 (4), 365–453.
Street, M., Baales, M., Gehlen, B., Heinen, M., Heuschen, W., Orschiedt, J., Schneid, N., Zander, A., 2019. Archaeology across the Pleistocene-Holocene boundary in western Germany : human responses to rapid environmental change. Préhistoire de l'Europe Dur Nord Ouest: Mobilités, Climats et Identités Culturelles 491–510.
Streif, H., 2004. Sedimentary record of Pleistocene and Holocene marine inundations along the North Sea coast of lower Saxony, Germany. Quat. Int. 112, 3–28.
Sturt, F., Garrow, D., Bradley, S., 2013. New models of north west European Holocene palaeogeography and inundation. J. Archaeol. Sci. 40, 3963–3976.
Surovell, T.A., Byrd Finley, J., Smith, G.M., Brantingham, P.J., Kelly, R., 2009. Correcting temporal frequency distributions for taphonomic bias. J. Archaeol. Sci. 36, 1715–1724.
Timpson, A., Colledge, S., Crema, E., Edinborough, K., Kerig, T., Manning, K., Thomas, M.G., Shennan, S., 2014. Reconstructing regional population fluctuations in the European Neolithic using radiocarbon dates: a new case-study using an improved method. J. Archaeol. Sci. 52, 549–557.
Torfing, T., 2015. Neolithic population and summed probability distribution of 14C-dates. J. Archaeol. Sci. 63, 193–198.
TNO-GDN, 2023. Geologische Kaart van het Koninkrijk der Nederlanden 1:600 000. TNO – Geologische Dienst Nederland. Geological Survey of the Netherlands), Utrecht.
Van der Molen, J., De Swart, H.E., 2001. Holocene wave conditions and wave-induced sand transport in the southern North Sea. Continent. Shelf Res. 21, 1723–1749.
Van de Plassche, O., 1982. Sea-level Change and Water-Level Movements in The Netherlands during the Holocene. Universiteit van Amsterdam.
Van der Plicht, J., Amkreutz, L.W.S.W., Niekus, M. J. L. Th, Peeters, J.H.M., Smit, B.I., 2016. Surf`n Turf in Doggerland: dating, stable isotopes and diet of Mesolithic human remains from the southern North Sea. J. Archaeol. Sci.: Reports 10, 110–118.
Van der Plicht, J., Kuitems, M., 2022. Fossil bones from the North Sea: radiocarbon and stable isotope (13C/15N) data. Radiocarbon 64, 633–668.
Van Geel, B., Van Der Plicht, J., Kasse, C., Mol, D., 2024. Radiocarbon dates from the Netherlands and Doggerland as a proxy for vegetation and faunal biomass between 55 and 5 ka cal bp. J. Quat. Sci. 39, 248–260.
Van Heteren, S., Meekes, J.A.C., Bakker, M.A.J., Gaffney, V., Fitch, S., Gearey, B.R., Paap, B.F., 2014. Reconstructing North Sea palaeolandscapes from 3D and high-density 2D seismic data: an overview. Neth. J. Geosci. 93, 31–42.
Van Maldegem, E., Vandendriessche, H., Verhegge, J., Sergant, J., Meylemans, E., Perdaen, Y., Lauryssen, F., Smolders, E., Crombé, P., 2021. Population collapse or human resilience in response to the 9.3 and 8.2 ka cooling events: a multi-proxy analysis of Mesolithic occupation in the Scheldt basin (Belgium). J. Anthropol. Archaeol. 64, 101348.
Vermeersch, P.M., 2011. The human occupation of the Benelux during the younger Dryas. Quat. Int. 242, 267–276.
Vermeersch, P.M., 2023. Comment on P.W. Hoebe, J.H.M. Peeters, S. Arnoldussen. Parsing prehistoric patterns: prospects and limitations of a big radiocarbon dataset for understanding the impact of climate on Late Palaeolithic and Mesolithic populations in northwest Europe (16–7.5 ka cal BP). J. Archaeol. Sci.: Reports 49, 103–944. Journal of Archaeological Science: Reports 52: 104054.
Vermeersen, B.L.A., Slangen, A.B.A., Gerkema, T., Baart, F., Cohen, K.M., Dangendorf, S., Duran-Matute, M., Frederikse, T., Grinsted, A., Hijma, M.P., Jevrejeva, S., Kiden, P., Kleinherenbrink, M., Meijles, E.W., Palmer, M.D., Rietbroek, R., Riva, R.E.M., Schulz, E., Slobbe, D.C., Simpson, M.J.R., Sterlini, P., Stocchi, P., van de Wal, R.S.W., van der Wegen, M., 2018. Sea-Level change in the Dutch wadden Sea. Neth. J. Geosci. 97, 79–127.
Vink, A., Steffen, H., Reinhardt, L., Kaufmann, G., 2007. Holocene relative sea-level change, isostatic subsidence and the radial viscosity structure of the mantle of northwest Europe (Belgium, The Netherlands, Germany, southern North Sea). Quat. Sci. Rev. 26, 3249–3275.
Vis, G., Cohen, K.M., Westerhoff, W.E., Veen, J.H.T., Hijma, M.P., Van Der Spek, A.J.F., Vos, P.C., 2015. Paleogeography. In: Long, I. Shennan A.J., Horton, B.P. (Eds.), Handbook of Sea-Level Research. Wiley, pp. 514–535.
Vos, P.C., Bunnik, F.P.M., Cohen, K.M., Cremer, H., 2015. A staged geogenetic approach to underwater archaeological prospection in the Port of Rotterdam (Yangtzehaven,

Maasvlakte, The Netherlands): a geological and palaeoenvironmental case study for local mapping of Mesolithic lowland landscapes. Quat. Int. 367, 4–31.
Waddington, C., 2015. A case for a secondary Mesolithic colonisation of Britain following rapid inundation of the North Sea Plain. In: Ashton, N., Harris, C.R.E. (Eds.), *No Stone Unturned: Papers In Honour Of Roger Jacobi*, Lithic Studies Society, pp. 221–232.
Waddington, C., Wicks, K., 2017. Resilience or wipe out? Evaluating the convergent impacts of the 8.2 ka event and Storegga tsunami on the Mesolithic of northeast Britain. J. Archaeol. Sci.: Reports 14, 692–714.
Waelbroeck, C., Labeyrie, L., Michel, E., Duplessy, J.C., McManus, J.F., Lambeck, K., Balbon, E., Labracherie, M., 2002. Sea-level and deep water temperature changes derived from benthic foraminifera isotopic records. Quat. Sci. Rev. 21, 295–305.
Walker, J., Gaffney, V., Fitch, S., Harding, R., Fraser, A., Muru, M., Tingle, M., 2022. The archaeological context of Doggerland during the final Palaeolithic and Mesolithic (chapter 5). In: Gaffney, V.G., Fitch, S. (Eds.), Europe's Lost Frontiers: Context and Methodology. Archaeopress Publishing, Oxford.
Ward, I., Larcombe, P., 2021. Sedimentary unknowns constrain the current use of frequency analysis of radiocarbon data sets in forming regional models of demographic change. Geoarchaeology 36, 546–570.
Ward, I., Larcombe, P., Lillie, M., 2006. The dating of Doggerland – post-glacial geochronology of the southern North Sea. Environ. Archaeol. 11, 207–218.
Weninger, B., Clare, L., Jöris, O., Jung, R., Edinborough, K., 2015. Quantum theory of radiocarbon calibration. World Archaeol. 47, 543–566.
Weninger, B., Schulting, R., Bradtmöller, M., Clare, L., Collard, M., Edinborough, K., Hilpert, J., Jöris, O., Niekus, M., Rohling, E.J., Wagner, B., 2008. The catastrophic final flooding of Doggerland by the Storegga Slide tsunami. Doc. praeh. 35, 1–24.
Williams, A.N., 2012. The use of summed radiocarbon probability distributions in archaeology: a review of methods. J. Archaeol. Sci. 39, 578–589.